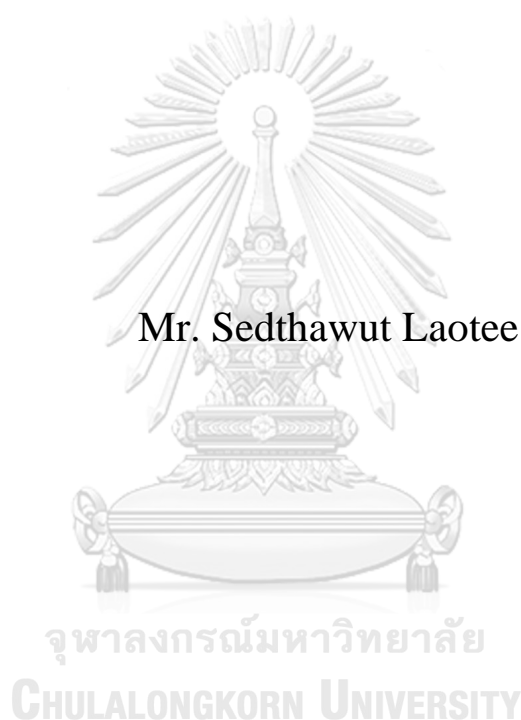


PRODUCTION AND CHARACTERIZATION OF
ESCHERICHIA COLI OUTER MEMBRANE VESICLES
DISPLAYING ANTI-MUC1 SINGLE-CHAIN VARIABLE
FRAGMENT VIA SPYTAG/SPYCATCHER SYSTEM



A Thesis Submitted in Partial Fulfillment of the Requirements
for the Degree of Master of Science in Pharmaceutical Sciences and
Technology
Common Course
FACULTY OF PHARMACEUTICAL SCIENCES
Chulalongkorn University
Academic Year 2021
Copyright of Chulalongkorn University

การผลิตและการแสดงลักษณะของถุงเยื่อหุ้มชั้นนอกของเอสเซอร์เรียโคไลที่มีชิ้นส่วนแปรผันสาย
เดี่ยวต่อมิวซินวันผ่านระบบสปายแท็ก/สปายแคทเซอร์



วิทยานิพนธ์นี้เป็นส่วนหนึ่งของการศึกษาตามหลักสูตรปริญญาวิทยาศาสตรมหาบัณฑิต
สาขาวิชาเภสัชศาสตร์และเทคโนโลยี ไม่สังกัดภาควิชา/เทียบเท่า
คณะเภสัชศาสตร์ จุฬาลงกรณ์มหาวิทยาลัย
ปีการศึกษา 2564
ลิขสิทธิ์ของจุฬาลงกรณ์มหาวิทยาลัย

เสถียร วุฒิ เหล่าที่ : การผลิตและการแสดงลักษณะของถุงเยื่อหุ้มชั้นนอกของเอสเชอริเชีย โคลิ ที่มีชั้นส่วน
 แปรผันสายเดี่ยวต่อมิวซินวันผ่านระบบสปายแท็ก/สปายแคทเชอร์. (PRODUCTION AND
 CHARACTERIZATION OF *ESCHERICHIA COLI* OUTER
 MEMBRANE VESICLES DISPLAYING ANTI-MUC1 SINGLE-
 CHAIN VARIABLE FRAGMENT VIA SPYTAG/SPYCATCHER
 SYSTEM) อ.ที่ปรึกษาหลัก : อ. ดร.วนัชร อรุณมณี, อ.ที่ปรึกษาร่วม : อ. ภก. ดร.นันทนเศรษฐ
 นลินรัตน์

เป็นเวลากว่าทศวรรษที่ถุงเยื่อหุ้มชั้นนอกจากเอสเชอริเชีย โคลิ ได้ถูกค้นพบ คุณสมบัติพิเศษเช่น ความคง
 ตัวสูง ความง่ายในการผลิต และคุณสมบัติในการเป็นสารเสริมฤทธิ์ ช่วยเน้นให้ถุงเยื่อหุ้มชั้นนอกถูกนำไปประยุกต์ใช้
 ในหลายด้าน เช่น วัคซีน สารช่วยให้มองเห็นและระบบขนส่งสารที่หลากหลาย จากวิธีการทางชีวสังเคราะห์สามารถ
 ทำให้ถุงเยื่อหุ้มชั้นนอกมีการแสดงโปรตีนจากสิ่งมีชีวิตอื่นด้วยการแสดงออกของโปรตีนลูกผสมของโปรตีนเป้าหมาย
 กับโปรตีนที่อยู่ที่ยู่อหุ้มชั้นนอก อย่างไรก็ตามโปรตีนที่มีโครงสร้างซับซ้อนอาจไม่สามารถถูกบรรจุไปยังถุงเยื่อหุ้ม
 ชั้นนอกได้ เนื่องจากในแบคทีเรียไม่มีการตัดแปลงโมเลกุลหลังการถอดรหัส ดังนั้นทางคณะผู้จัดทำได้เสนอวิธีที่
 สะดวกในการแสดงออกโปรตีนที่หลากหลายในถุงเยื่อหุ้มชั้นนอก ด้วยการประยุกต์ใช้จากระบบเชื่อมต่อทางชีววิทยา
 ชื่อว่าสปายแท็ก/สปายแคทเชอร์ ถุงเยื่อหุ้มชั้นนอกที่สังเคราะห์จากเอสเชอริเชีย โคลิ ถูกผลิตให้ติดสปายแคทเชอร์ผ่าน
 ระบบแสดงออกบนผิวเซลล์ Lpp'OmpA (OMVs:Lpp'OmpA-SpyCatcher) เพื่อทดสอบต้นแบบ
 ของการติดโปรตีนบนถุงเยื่อหุ้มชั้นนอก ชั้นส่วนแปรผันสายเดี่ยวต่อมิวซินวันชนิด SM3 ซึ่งถูกใช้การจดจำ
 เซลล์มะเร็งที่มีการแสดงออกของมิวซินวันนั้น ได้ถูกเลือกเพื่อนำมาผลิตในรูปแบบของโปรตีนลูกผสมกับสปายแท็ก
 (SpyTag-SM3) ในเซลล์รังไข่ของหนูแฮมสเตอร์ซึ่งมีการตัดแปลงโมเลกุลหลังการถอดรหัสด้วยพันธะได
 ซัลไฟด์เพื่อรักษาหน้าที่ของชั้นส่วนแปรผันสายเดี่ยวดังกล่าว ภายหลังจากผสมสปายแท็กจะเกิดพันธะไอโซเปปไทด์
 อย่างว่องไวและผันกลับไม่ได้กับสปายแคทเชอร์ซึ่งทำให้สามารถต่อ SpyTag-SM3 เข้ากับ
 OMVs:Lpp'OmpA-SpyCatcher ได้ จากการตรวจสอบด้วย Western blot พบว่าสามารถยืนยัน
 ตัวตนของผลิตภัณฑ์จากการเชื่อมต่อได้ คุณลักษณะทางเคมีกายภาพของถุงเยื่อหุ้มชั้นนอกที่ถูกเชื่อมต่อได้ถูกวิเคราะห์
 ด้วย Dynamic light scattering และ Transmission electron microscope จากการติดกับ
 โปรตีน SM3 นั้นทำให้พบว่าลักษณะพื้นฐานวิทยาของถุงเยื่อหุ้มชั้นนอกที่ถูกติดนั้นมีลักษณะเป็นถุงไขมันทรงกลมและมี
 ขนาด 103.77 นาโนเมตร นอกจากนั้นคณะผู้จัดทำสามารถยืนยันตำแหน่งของโปรตีน SM3 บนผิวของถุงเยื่อ
 หุ้มชั้นนอกได้โดยใช้วิธีวิเคราะห์การป้องกันการย่อยของ proteinase K และจากผลทดสอบการจับต่อเซลล์ที่มี
 การแสดงออกของมิวซินวัน (MCF-7) ได้ชี้ให้เห็นถึงความสามารถในการจับของชั้นส่วนแปรผันสายเดี่ยวต่อมิว
 ซินวันชนิด SM3 ที่ถูกแสดงอยู่บนผิวของถุงเยื่อหุ้มชั้นนอกที่ถูกเชื่อมต่อ จากผลสรุปรายงานนี้ได้นำเสนอระบบการ
 ตกแต่งโปรตีนที่ปรับเปลี่ยนได้ง่ายบนถุงเยื่อหุ้มชั้นนอกซึ่งสามารถนำไปใช้ในระบบขนส่งยาที่มีความจำเพาะระดับ
 เซลล์ได้

สาขาวิชา เกษศาสตร์และเทคโนโลยี

ลายมือชื่อนิติ

ปีการศึกษา 2564

ลายมือชื่อ อ.ที่ปรึกษาหลัก

ลายมือชื่อ อ.ที่ปรึกษาร่วม

6270033833 : MAJOR PHARMACEUTICAL SCIENCES AND TECHNOLOGY

KEYWORD: Outer membrane vesicle, Mucin 1, SpyTag/SpyCatcher system, Single-chain variable fragment, Targeted drug delivery system

Sedthawut Laotee : PRODUCTION AND CHARACTERIZATION OF *ESCHERICHIA COLI* OUTER MEMBRANE VESICLES DISPLAYING ANTI-MUC1 SINGLE-CHAIN VARIABLE FRAGMENT VIA SPYTAG/SPYCATCHER SYSTEM. Advisor: WANATCHAPORN ARUNMANEE, Ph.D. Co-advisor: NONTHANETH NALINRATANA, Ph.D.

Outer membrane vesicles (OMVs) secreted from Gram-negative bacteria have been discovered for a decade. Special features like high stability, ease of production, and intrinsic adjuvanticity highlight the use of OMVs in diverse applications such as vaccination, bioimaging, and multifunctional delivery systems. Synthetic biological approaches can functionalize OMVs to present heterologous proteins by expressing genetic fusion of target protein to outer membrane proteins. However, complex proteins cannot be incorporated into the OMVs due to lack of some post-translational modifications in bacteria. Herein, we demonstrated a convenient method for presentation of versatile proteins in OMVs with the implementation of the bio-ligation system called SpyTag/SpyCatcher system. OMVs derived from *Escherichia coli* were generated to anchor SpyCatcher via Lpp'OmpA surface display system (OMVs:Lpp'OmpA-SpyCatcher). To test the proof-of-concept, anti-MUC1 single-chain variable fragment (scFv) clone SM3 which previously used in targeting MUC1-presenting tumor cells was chosen and produced as a fusion with SpyTag (SpyTag-SM3) in CHO-based expression system. This system provides disulfide linkage processes to maintain its function. Upon mixing, SpyTag simultaneously performs an irreversible isopeptide bond with SpyCatcher resulting in coupling of SpyTag-SM3 onto the surface of OMVs:Lpp'OmpA-SpyCatcher. The conjugation of two proteins on OMVs was confirmed by Western blotting. Physicochemical characterizations of conjugated OMVs were also analyzed by Dynamic light scattering and Transmission electron microscope. Despite attachment of anti-MUC1 scFv SM3, the morphology of conjugated OMVs was spherical lipid vesicles with the size of 103.77 nm. In addition, the localization of scFv SM3 was observed on the surface of the OMVs as evaluated by proteinase K protection assay. Furthermore, the result of binding analysis towards MUC1-presenting cell (MCF-7) indicated the binding of anti-MUC1 scFv SM3 displayed on the conjugated OMVs. As a result, this study provides a flexible protein decoration system in OMVs that can be used in targeted drug delivery system.

Field of Study:	Pharmaceutical Sciences and Technology	Student's Signature
Academic Year:	2021	Advisor's Signature
		Co-advisor's Signature

ACKNOWLEDGEMENTS

First of all, I would like to express my deepest gratitude to my thesis advisor, Wanatchaporn Arunmanee, Ph.D. for supervision of this study as well as her guidance, encouragement, and providing me opportunities to explore the world. I cannot thank her enough for what she has done for me over these years.

My gratefulness extends to my co-advisor, Nonthaneth Nalinratana, Ph.D. for his help and suggestion for cell-based assays. In addition, I would also like to thank thesis committees including Asst. Prof. Chatchai Chaotham, Ph.D., Asst. Prof. Jittima Amie Luckanagul, Ph.D., and Pinpunya Riangrunroj, Ph.D. for their advice in my study.

Next, I would like to give my sincere thanks to the staff of Department of Biochemistry and Microbiology, Faculty of Pharmaceutical Sciences, Chulalongkorn University and the faculty staff for their help and assistance.

As a member of S3Bio Lab where I have experienced lots of memorable moments, I am thankful to all members for teaching me, suggesting me, and cheering me up throughout the years. Plus, the students of the Department of Biochemistry and Microbiology are acknowledged because of their never-ending support and caring.

My greatest appreciation belongs to my family members who are always beside me. I would like to thank them for believing in me and sending me unconditional love.

Also, my gratitude is owed to Chulalongkorn University for my Research Assistant Scholarship and financial support of this research from the 90th Anniversary of Chulalongkorn University Fund (Ratchadaphiseksomphot Endowment Fund).

Finally, I would like to thank my lovely friends that have always been supporting me and those who are not mentioned that contribute to my work. Last but not the least, I would like to give a kind reminder to those who are chasing their dreams that I, who almost gave up several times, can make this work real. Thus, just remember that if I can do it, so can you.

Sedthawut Laotee

TABLE OF CONTENTS

	Page
ABSTRACT (THAI)	iii
ABSTRACT (ENGLISH).....	iv
ACKNOWLEDGEMENTS.....	v
TABLE OF CONTENTS.....	vi
LIST OF TABLES.....	vii
LIST OF FIGURES	viii
LIST OF ABBREVIATIONS.....	1
CHAPTER I INTRODUCTION.....	2
CHAPTER II LITERATURE REVIEW	6
CHAPTER III MATERIALS AND METHODS	21
CHAPTER IV RESULTS.....	33
CHAPTER V DISCUSSION AND CONCLUSION	46
REFERENCES	51
APPENDIX.....	59
VITA.....	67

LIST OF TABLES

	Page
Table 1 Current protein display systems in OMVs.....	9
Table 2 Components of conjugated OMVs in various ratios.....	28



LIST OF FIGURES

	Page
Figure 1 Biogenesis of OMVs in Gram-negative bacteria.....	7
Figure 2 Mechanisms of OMVs that mediate immune cells.....	8
Figure 3 Flow chart of Omp22 presentation on OMVs using ClyA fusion system....	12
Figure 4 Schematic representation of Lpp'OmpA fused with protein of interest.....	13
Figure 5 Ribbon structure of SpyTag/SpyCatcher.....	15
Figure 6 The structure of Mucin 1 in normal epithelial cells and tumor cells.....	18
Figure 7 Three-dimensional structure of anti-MUC1 scFv clone SM3	20
Figure 8 Schematic representation of expression plasmids used in this study	34
Figure 9 Colony PCR analysis of pLpp'OmpA-SpyCatcher transformants.....	35
Figure 10 Colony PCR analysis of pSpyTag-SM3 from transformed colonies.....	35
Figure 11 Expression and localization of Lpp'OmpA-SpyCatcher	36
Figure 12 The chromatogram of SpyTag-SM3 purified from the supernatant of transfected cells.....	38
Figure 13 Identification of purified SpyTag-SM3 by SDS-PAGE analysis and Western blot	38
Figure 14 Optimization of conjugation ratio of OMVs:Lpp'OmpA-SpyCatcher and SpyTag-SM3	40
Figure 15 SpyTag/SpyCatcher ligation of SpyTag-SM3 to OMVs:Lpp'OmpA-SpyCatcher evaluated by immunoblotting analysis.....	40
Figure 16 Size distribution profile of the vesicles determined by Dynamic light scattering	41
Figure 17 Transmission electron microscopic images of uranyl acetate-stained OMVs samples.....	42
Figure 18 SDS-PAGE and Western blotting analysis presenting proteinase K protection assay of scFv SM3-presenting OMVs	43
Figure 19 Gold-labelled TEM images	44
Figure 20 Binding activity of OMVs samples and scFv SM3 in MCF-7 cells evaluated by cell-based ELISA.....	45

Figure 21 The circular map of pET21a+ vector.....	60
Figure 22 Sequence of gene cassette encoding Lpp'OmpA-SpyCatcher	61
Figure 23 DNA sequence alignment of designed Lpp'OmpA-SpyCatcher sequence	62
Figure 24 The circular map of pFUSE-hIgG1-Fc2.....	63
Figure 25 DNA sequences of genes used in Gibson assembly for construction of pSpyTag-SM3	64
Figure 26 SpyTag-SM3 DNA coding sequence and amino acid sequence	65
Figure 27 DNA alignment of sequencing read from recombinant pSpyTag-SM3.....	66



LIST OF ABBREVIATIONS

α	Alpha
β	Beta
BCA	Bicinchoninic acid
Da	Dalton
kDa	Kilodalton
$^{\circ}$	Degree
$^{\circ}\text{C}$	Degree Celsius
g	Gram
mg	Milligram
ng	Nanogram
μg	Microgram
h	Hour
kV	Kilovolt
L	Liter
mL	Milliliter
μL	Microliter
mA	Milliamp
mm	Millimeter
min	Minute
n	Number
OD	Optical density
pmol	Picomole
nm	Nanometer
rpm	Revolutions per minute
s	Second

CHAPTER I

INTRODUCTION

Outer membrane vesicles (OMVs) are spherical vesicles with bilayer structure of bacterial outer membrane. As reported by previous studies, diameter size of OMVs is ranging from 20 to 200 nm depending on species of bacteria (1, 2). OMVs are generated by budding of outer membrane from Gram-negative bacteria using unclear mechanisms (3). Generally, roles of OMVs are involved in bacterial communication, bacteria-host interaction, triggering biofilm formation, delivery of toxins, horizontal gene transfer, stress responses and so on (4, 5). Common components in OMVs are included of lipopolysaccharide (LPS), outer membrane proteins (OMPs), periplasmic proteins, lipids, and nucleic acids (3). Because of some biomolecules in OMVs such as LPS, virulent factors, and toxins, naturally-secreted OMVs from pathogenic bacteria can serve as a vaccine against parental bacteria (6). For example, a multi-component vaccine including *Neisseria meningitidis*-derived OMVs has been approved by United States of Food and Drug Administration (U.S. FDA) to control serogroup B meningococcal disease in a combination with other three purified compounds from *N. meningitidis* named as '4CMenB' or 'BEXSERO' (7). This highlights an attractive use of OMVs as a vaccine platform.

Among nano-sized particles available in the present, outer membrane vesicles (OMVs) feature superior advantages to utilize in several applications including high stability, ease of production, and built-in adjuvanticity (8, 9). Apart from native OMVs, OMVs from non-pathogenic bacteria can be modified to carry heterologous proteins using genetic engineering approaches. These bioengineered OMVs have been utilized in diverse applications such as a vaccination, a delivery platform of a wide variety of molecules, and a bioimaging (10-13). Incorporation of heterologous proteins in OMVs relies on a genetic fusion of target protein with periplasmic signal peptides such as signal peptide of outer membrane protein A (OmpA), or outer membrane-associated proteins such as cytolysin A (ClyA) and hemoglobin protease (Hbp) (14-16). On the other hand, packaging target protein into OMVs using these previous carriers is limited for proteins that suits to bacterial expression. Owing to lack of post-translational

modifications including glycosylation and disulfide linkage, target proteins that require complex modifications have to be expressed together with production of OMVs resulting in loss of native structure and function. Hence, development of a method for presentation of various proteins in OMVs is challenging.

To overcome this problem, separated production of OMVs and target protein is preferably performed followed by joining them together via bio-conjugation. One of the protein-protein ligation methods is the SpyTag/SpyCatcher system which is a bio-ligation system consisting of SpyTag, a 13 amino acid peptide, and 15 kDa protein, SpyCatcher, previously derived from fibronectin binding protein (FbaB) of *Streptococcus pyogenes*. These two protein partners can form simultaneous linkage through an irreversible isopeptide bond that remains stable in various conditions. Additionally, SpyTag and SpyCatcher can be genetically fused to proteins of interest at N-terminus, C-terminus, and internal positions (17, 18). These advantages prompted researchers to apply them in heterologous protein decoration on variety of nanoparticles such as virus-like particle (VLP), Gram-positive enhance matrix particle (GEM), and yeast ghost shell (19-21).

To validate the proof-of-concept of this decoration system and enhance functionality of our bioengineered OMVs, we aimed to generate cancer-targeting OMVs by decorating OMVs with an antibody fragment against cancers. Mucin 1 (MUC1) glycoprotein was chosen as a target molecule for targeting cancer cells as it is overexpressed and has altered glycosylated pattern in several cancer cells including breast cancer, colon cancer, and pancreatic cancer (22, 23). Also, previous report demonstrated that MUC1 enables internalization of drugs upon binding with drug-conjugated targeting molecule (24, 25). As these reasons combined, MUC1 is potentially serving as a target for drug delivery in cancer therapy. Several monoclonal antibodies targeting cancer-associated MUC1 were identified such as HMFG-2 and SM3 (26, 27). Even though anti-MUC1 antibody clone SM3 showed lower affinity to MUC1 epitope compared to HMFG2, it exhibited weak interaction towards normal cells and benign tumor while HMFG2 still reacts to normal cells supporting the use of anti-MUC1 antibody clone SM3 as MUC1-targeting molecule (28).

Production of MUC1-targeting OMVs was conducted by conjugation of OMVs presenting SpyCatcher and SpyTag-fused anti-MUC1 antibody clone SM3. SpyCatcher was incorporated into the *Escherichia coli*-derived OMVs via a genetic fusion of Lpp'OmpA. The Lpp'OmpA system is well-known bacterial display system consisting of the first nine amino acid of *E. coli* major lipoprotein and *E. coli* outer membrane protein A (OmpA) residue 46 - 159 (29). This system was utilized for heterologous protein display in numerous applications (30-32). Expression of SpyTag-fused single chain variable fragment (scFv) derived from anti-MUC1 antibody clone SM3 was performed in CHO-based expression system that provides disulfide bond formation to retain its structural integrity (33). After purification processes, SpyTag-fused anti-MUC1 scFv clone SM3 was coupled to OMVs presenting SpyCatcher. Subsequently, the bio-ligation reaction was confirmed, and physicochemical properties of the conjugated OMVs were characterized. Next, presence of anti-MUC1 scFv clone SM3 on the surface of the OMVs was validated and binding activity against MUC1-presenting cell was verified. Our study will benefit versatile protein decoration in OMVs development and OMVs-based cell-specific drug delivery.

Research question

Can recombinant anti-MUC1 scFv (SM3) be attached on the surface of *E. coli*-derived outer membrane vesicles via SpyTag/SpyCatcher system?

Objectives

1. To produce outer membrane vesicles from *E. coli* displaying anti-MUC1 scFv (SM3) via SpyTag/SpyCatcher system
2. To characterize physicochemical properties of outer membrane vesicles from *E. coli* and validate the presence of anti-MUC1 scFv (SM3) on the surface of the vesicles

Hypothesis

Recombinant anti-MUC1 scFv (SM3) can be attached on the surface of *E. coli*-derived outer membrane vesicles utilized by SpyTag/SpyCatcher system.

Expected benefits

This study provides a convenient method for decoration of versatile proteins on *E. coli*-derived outer membrane vesicles that can be used as a targeted drug delivery system.



CHAPTER II

LITERATURE REVIEW

1. Bacterial outer membrane vesicles

1.1. Biogenesis and pathogenic functions

Outer membrane vesicles (OMVs) are a non-replicative nanoscale spherical proteoliposome secreted by Gram-negative bacteria. The size of OMVs is ranging around 20 to 200 nm depending on species of bacteria. A unique characteristic of OMVs is a bilayer structure that is derived from outer membrane of parental bacteria. Common constituents found in OMVs are outer membrane-associated compounds such as LPS, OMPs, periplasmic contents, lipids, nucleic acid, and virulence factor (1-4). Mechanisms of OMVs generation are complex and remain unclear (34). One of the proposed mechanisms is loss of linkages between outer membrane and peptidoglycan mediated by lipoproteins that can initiate bulging of outer membrane resulting in OMVs vesiculation (35, 36). This model is elucidated by increase of OMVs production in mutant *E. coli*, *Salmonella spp.*, and *Acinetobacter baumannii* that lacks outer membrane protein A (OmpA) (4). OmpA is known to involve in crosslink of peptidoglycan and outer membrane, so an absence of OmpA affects decrease of the crosslink leading to increased OMVs production (37). As well as lipoproteins, lipid-binding molecules have been studied to be involved in OMVs release. For example, *Pseudomonas quinolone signal* (PQS), an LPS-binding molecule, can alter LPS expansion symmetry triggering OMVs production. However, this assumption is limited to *Pseudomonas aeruginosa*, suggesting a specie-specific mechanism of OMVs generation (38). Biological functions of OMVs take place in numerous bacterial activities including bacterial physiology, bacterial communication, nutrient acquisition, horizontal gene transfer, and stress responses (1-4). For instance, in response to stresses caused by accumulated misfolded proteins, bacteria transport those proteins into the OMVs and drive secretion of the vesicles to reduce intracellular turgor pressure (figure 1) (39). Apart from removal of protein waste, bacterial OMVs also play an essential role in pathogenesis by delivering toxin and virulence factors to host cells (5, 34). In addition, OMVs could interact with the host cells causing miserable events such as

morphology change, induction of inflammatory responses (2). As previously discussed, OMVs can internalize into host cells via diverse mechanisms including endocytosis mediated by clathrin or caveolin, lipid raft, and membrane fusion. Importantly, OMVs can mediate epithelial cells and pass over epithelial barrier resulting in recruitment of immune-related cells (figure 2) (40). It has been known that LPS contained in OMVs is considered as pathogen-associated molecular pattern (PAMP) which can be recognized by pattern recognition receptors (PRRs) in immune cells (1-5). As a result, the effects of OMVs in host cells after internalization to submucosa site have been intensively discussed. For example, OMVs from *N. meningitidis* can activate neutrophils to produce inflammatory cytokines including tumor necrosis factor alpha (TNF- α), interleukin 1 beta (IL-1 β) and upregulate expressions of CXCL8 and CCL4 (41). Similar phenomenon is also observed in OMVs from other bacteria including *Legionella pneumophila*, *Helicobacter pylori*, and *E. coli* (5).

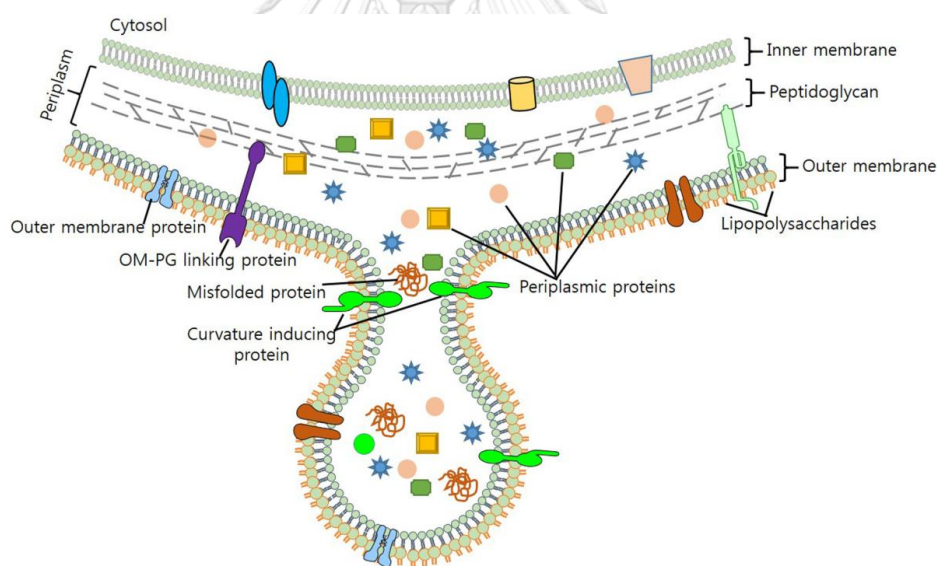


Figure 1 Biogenesis of OMVs in Gram-negative bacteria(3)

1.2. Uses of naturally secreted OMVs

Based on their origin, bacterial OMVs can be divided into two types: naturally secreted OMVs and bioengineered OMVs. For native OMVs, they have been used in two main applications including a vaccine platform and a drug delivery system. As a vaccine delivery vehicle, OMVs isolated from pathogenic bacteria can deliver specific

antigen to host immune cells and trigger immune responses to provide protection against the parental bacteria. Combined with adjuvanted properties, native OMVs could strongly boost immunogenicity of the partner antigen indicating OMVs as a promising vaccine delivery platform (6). For instance, Marina R. Pulido demonstrated that OMVs budded from *Acinetobacter baumannii* could elicit robust humoral immune responses and provide protection against actual *A. baumannii* infection (42). Moreover, OMVs vaccine (known as '4CMenB' or 'BEXERO') from *Neisseria meningitidis* has been approved by U.S. FDA to control serogroup B meningococcal disease in a combination with other three purified compounds from *N. meningitidis* (7). Not only the native OMVs can serve as a vaccine delivery platform, but they also can act as a drug vehicle due to preferable features like rigid structure which can avoid drug leakage. As demonstrated by Kudelaidi Kuerban and team, *Klebsiella pneumoniae*-derived OMVs were loaded by a neoplastic agent, doxorubicin, and used to treat non-small lung cancer cells (43). The results showed that doxorubicin could be delivered to cancer cells when loaded in OMVs, as evaluated in in vitro and in vivo models. Moreover, proper immunogenicity of OMVs could activate recruitment of macrophage that can enhance effectiveness of tumor clearance by doxorubicin-loaded OMVs.

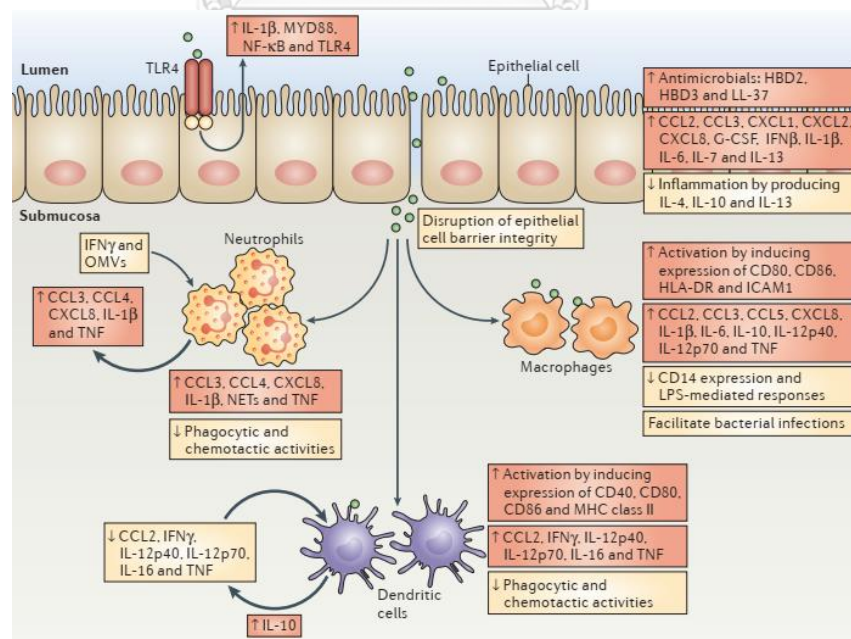


Figure 2 Mechanisms of OMVs that mediate immune cells(9)

1.3. Bioengineered OMVs and their applications

In contrast to naturally secreted OMVs, OMVs budded from non-pathogenic bacteria can be utilized in diverse applications by modifying phenotypes using genetic engineering approaches. Among species of bacteria, *E. coli* is considered as an effective bacterial factory for OMVs production because of its well-tolerance to genetic engineering processes, simple cultivation, and cost-effective production. Strains of *E. coli* used in production of bioengineered OMVs are consisting of common strains like DH5 α , BL21(DE3), hyper-vesiculated strains like JC8031 (14, 44, 45). One attempt to modify the OMVs is to load heterologous proteins onto OMVs via genetic fusion with OMV-associated proteins. Based on compartments of OMVs, target protein can be packaged within production of OMVs and consequently exported into the lumen or exposed on the surface (6, 34, 45). To incorporate heterologous protein into the lumen of OMVs, the target protein is fused to signal peptides that facilitated protein sorting to periplasm space such as the signal peptide of outer membrane protein A (OmpA), Tat signal sequence, OprI lipoprotein (16, 46-48). On the contrary, membrane-bound proteins like *E. coli* Cytolysin A (ClyA), Hemoglobin-binding protease (Hbp), and well-known bacterial surface display system (Lipoprotein-OmpA hybrid, Lpp'OmpA) have been demonstrated to display heterologous protein in surface-exposed manner (14, 15, 49). In the present, current protein display systems in OMVs are listed in table 1.

Table 1 Current protein display systems in OMVs

Carrier	Protein of study	Location of target protein	Limitation	Ref.
Original systems				
OmpA	FLAG	Lumen	-	(10)
The signal peptide of OmpA	SpyCEP, Streptolysin O, Spy0269, and SAM_1372	Lumen	-	(16)
	HtrA			(48)
Tat signal	GFP	Lumen	-	(46)
Maltose binding protein (MBP)	mD8-FAT	Lumen	-	(50)

Hbp	ESAT6, Ag85B fragment, and Rv2660c	Surface exposure	Performance is depended on size and complexity of target protein	(15)
OprI lipoprotein	A104R antigen	Surface exposure	Structure of target protein may be changed by purification steps	(47)
ClyA	Affibody against HER2	Surface exposure	Possible toxicity of hemolysin activity of ClyA	(10)
	GFP			(14, 51)
	Anti-digoxin scFv			(14)
	Omp22			(45)
	GalT			(52)
	M2e			(53)
Lpp'OmpA	Histidine-tag	Surface exposure	Performance is depended on size and complexity of target protein	(49)
Utilized with SpyTag/SpyCatcher system				
OmpA fused to SpyCatcher	PTE	Lumen	Digested products occurred from proteolysis	(44)
Hbp fused to either SpyTag or SpyCatcher	SP1690 fusion and anti-GFP nanobody	Surface exposure	Amount of antigen	(54)
	TrxA and MBP			(55)
ClyA fused to SpyCatcher	Ovalbumin	Surface exposure	Possible toxicity of hemolysin activity of ClyA	(56)
Lpp'OmpA fused to SpyCatcher (This study)	Anti-MUC1 scFv clone SM3	Surface exposure	Suboptimal protein display	-

Similar to native OMVs, bioengineered OMVs can act as an antigen delivery system as described in many reports (45, 47, 50-53, 56). An idea of using bioengineered

OMVs as a vaccine platform is illustrated by fusion protein of antigenic protein from the pathogen and the protein carriers. One of the most common protein display systems is ClyA system. This pore-forming hemolytic protein has shown to be located in *E. coli*-derived OMVs and enables transportation of its C-terminal fusion partner to the surface of OMVs (14, 45, 51-53). It has been firstly demonstrated by Jae-Young Kim and team that green-fluorescent protein (GFP) could be incorporated into OMVs by fusing to ClyA (14). The ClyA system aids development of OMVs-based vaccines in several studies. For example, Weiwei Huang generated bioengineered *E. coli* OMVs displaying immunogenic outer membrane protein of *A. baumannii* (Omp22) and immunized recombinant OMVs to mice as shown in figure 3 (45). The results indicated that Omp22-displaying OMVs could trigger a robust immune responses that protected mice from challenge of *A. baumannii*. Likewise, a truncated cancer antigen, D8 region from mouse FAT atypical cadherin 1 (mD8-FAT1) which is abundantly expressed on colorectal cancers, was packaged into *E. coli*-derived OMVs serving as a vaccination for cancer treatment (50). Unlike ClyA system that transports target protein to the surface, Alberto Grandi and team engineered OMVs to present mD8-FAT1 inside the lumen via fusing to *E. coli* MBP located in periplasm. The resulting OMVs could activate production of anti-mD8-FAT1 antibodies and partially protected immunized mice from tumor challenge. Notably, the choice of production of OMVs-based vaccines is still debatable that which location of antigen is preferable to prime immune system. While surface-exposed manner provides accessibility to be captured by immune cells, at the same time, is easily degraded by serum proteases (6). On the other hand, safer delivery of antigen by packing into the lumen of OMVs is more appreciated, but an inadequate immune response may be found.

Bioengineered OMVs also showed capability to deliver various compounds to the host cells. For example, Vipul Gujrati and team illustrated an alternative approach to enhance ability of the bioengineered OMVs as a multifunctional delivery platform. They created bioengineered OMVs from *E. coli* to carry melanin. Accumulation of melanin in the lumen of OMVs was made by heterologous expression of *Rhizobium etli* tyrosinase which catalyzes in melanin biosynthesis (57). The melanin-loaded OMVs were applied to utilized as an optoacoustic imaging in cancer treatment. In addition,

combining protein display system and cargo delivery ability, bioengineered OMVs prompts us to use them as a targeted delivery platform. Previous study showed that target-specific OMVs were generated by displaying affibody against HER2 via ClyA fusion system (10). HER2 is overexpressed in various tumor cells, so affibody against HER2 that is decorated on OMVs can transport selectively to HER2-presenting cells. After production of HER2-specific OMVs, a small interfering RNA (siRNA) targeting kinesin spindle protein (KSP) was loaded to the OMVs aiming to reduce cancer growth. As performed in both in vitro and in vivo models, siRNA in HER-targeting OMVs could specifically down-regulate its target leading to regression of tumor cells and non-specific side-effects were not found in both in vitro and in vivo models. Collectively, bioengineering of OMVs could improve efficacy of native OMVs to use in various purposes.

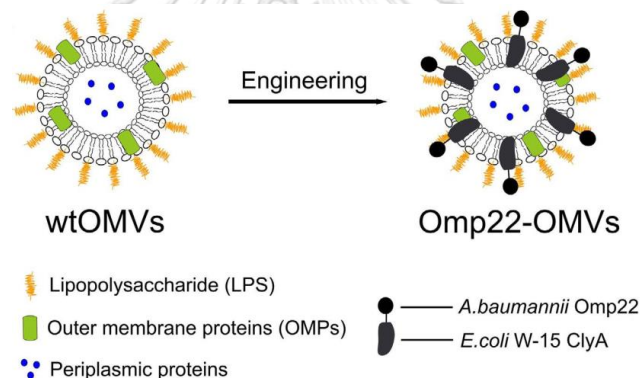


Figure 3 Flow chart of Omp22 presentation on OMVs using ClyA fusion system(45)

2. Lpp'OmpA as a bacterial surface display system

The Lpp'OmpA hybrid is one of well-known bacterial display systems. It has been firstly discovered by Joseph A. Francisco and team in an attempt to anchor β -lactamase on outer membrane of *E. coli* (29). The system is consisting of two major components: 1) The first nine residue of *E. coli* lipoprotein which acts as signal peptide to translocate to periplasm space and subsequently integrate into outer membrane via N-terminal cysteine modified with diglyceride and fatty acid moieties (58, 59) and 2) The truncated outer membrane protein A (OmpA) including residue 46 – 159 containing five membrane-spanning β -sheet domains and surface-exposed C-terminal tail (60).

This Lpp'OmpA chimera allows its C-terminal fusion partner to display on bacterial surface. Various proteins have been successfully displayed by this system and utilized in various applications such as whole-cell biocatalyst, scFv screening system, and simplified protein purification tool (figure 4) (29, 31, 32, 60). For example, functional *Bacillus licheniformis* lipase was successfully expressed and located on the surface of *E. coli*. The function of lipase anchored on bacterial surface was confirmed by enzymatic activity assay towards the substrates, *p*-nitrophenyl caprylate (31). Moreover, as a selection tool for scFv discovery, the Lpp'OmpA was fused to anti-digoxin, a fluorescent-labelled hapten, scFv libraries to isolate high-affinity and subjected to screening processes using fluorescence-activated cell sorting (FACS). The resulting scFv was later purified and showed a convincing binding activity to the ligand (60). Despite successful surface exposure of a variety of proteins, one consideration of using the Lpp'OmpA system is the performance of protein display is depending on its fusion size and complexity. As illustrated by Costas Stathopoulos and team, fusing Lpp'OmpA to an alkaline phosphatase (PhoA) which is large (94 kDa) and has complex structure could not be translocated to the bacterial membrane (30).

To apply Lpp'OmpA hybrid in protein display system of OMVs, Jae-Young Kim and team have demonstrated that a protein with complex structure like anti-digoxin scFv could not be incorporated in the OMVs by using this system (14). However, as illustrated by Nathan J. Alves and team, histidine-tagged Lpp'OmpA could be targeted into OMVs to allow purification of desired vesicles by using the Ni-NTA affinity chromatography (49). As a result, it indicates that size and complicated structure can affect significantly to presentation of target protein on OMVs.

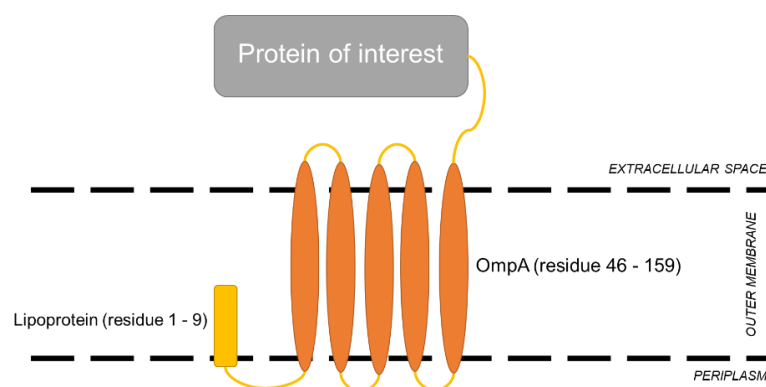


Figure 4 Schematic representation of Lpp'OmpA fused with protein of interest

3. Efficient bio-ligation system of SpyTag/SpyCatcher

SpyTag/SpyCatcher system is a bioconjugation system comprising of two protein partners performing an irreversible isopeptide bond. This system was derived from *Streptococcus pyogenes* fibronectin-binding protein (FbaB) which contains intracellular interaction. Bijan Zakeri and team found that the second immunoglobulin-like collagen adhesin domain (CnaB2) in *S. pyogenes* FbaB can perform a covalent bond between Lysine (residue 31, Lys³¹) and Aspartic acid (residue 117, Asp¹¹⁷) (17). As shown in the same study, the isopeptide bond is formed by nucleophilic attack of Asp¹¹⁷ by Lys³¹ which is catalyzed by neighbor Glutamic acid (residue 77, Glu⁷⁷). Consequently, they reconstructed two protein fragments: a short peptide (SpyTag), 13 amino acids consisting of Asp¹¹⁷, and its protein partner (SpyCatcher), ~15 kDa containing Lys³¹ (figure 5). The rate constant of SpyTag/SpyCatcher reaction was achieved about $1.4 \times 10^{-3} \text{ M}^{-1} \text{ s}^{-1}$, indicating a rapid formation that is beneficial to practical usage. Additionally, the bond formation of SpyTag/SpyCatcher could retain stability in diverse conditions (pH, temperature, and buffer). Furthermore, due to flexibility to genetically fuse to target proteins, SpyTag/SpyCatcher system has been utilized in coupling two individual proteins as demonstrated in various reports (19-21, 61, 62). SpyTag and SpyCatcher could be independently fused to the protein of interest at various sites (either N-terminus, C-terminus, interval site, or loop structure) and showed no loss of ligation efficacy (63).

Owing to these benefits, SpyTag/SpyCatcher system has been applied in a wide range of applications such as enzyme fabrication, biomolecule delivery system, synthetic bacterial compartment, and so on (18-21, 61, 62). Aside from those applications, the most favored utilization of SpyTag/SpyCatcher system is to attach antigen on the surface of nanoparticles like VLP, GEM, and yeast ghost shell (YGS), termed it as a Plug-and-Display approach (19-21). This effort was primarily validated by displaying SpyTag-fused malaria antigens (CIDR and Pfs25) on SpyCatcher-expressed in the surface of *E. coli*-derived VLPs from the bacteriophage AP205. After that, the resulting VLPs were injected to mice and elicited robust antibody responses (19). Likewise, the SpyTag/SpyCatcher system was used to decorate the yeast-derived β -glucan microparticles (YGS) serving as an immune-booster device of *Actinobacillus*

pleuroneumoniae antigen (ApxIA) and robust immune responses were shown in immunized mice, suggesting an ideal use of SpyTag/SpyCatcher for vaccine platform (20).

With the intention of using SpyTag/SpyCatcher system in OMVs development, published reports have illustrated to present various proteins including bacteria antigen, tumor neoantigen, nanobody. Similar to other nano-sized particles, the SpyTag/SpyCatcher system was utilized in display of protein of interest on OMVs by fusing either SpyTag or SpyCatcher to carriers (such as ClyA and Hbp) and target protein (54-56). For instance, OMVs displaying anti-GFP nanobody were generated by linking SpyCatcher-fusion of the nanobody and engineered Hbp which its domain 1 was replaced by SpyTag (54). Unlike surface display strategy mediated by ClyA or Hbp, SpyTag/SpyCatcher system could also sort protein into the lumen of OMVs as illustrated by Nathan J. Alves and team. The lumen-located enzyme packaging in OMVs was performed by linking C-terminal fusion of OmpA to SpyTag and SpyCatcher-linked *Brevundimonas diminuta* Phosphotriesterase (PTE). This enzyme was shown to be packaged in the lumen of OMVs and could retain its catalytic activity. The benefit of loading the enzyme into OMVs is to increase stability as demonstrated by lower degree of degradation compared to the free enzyme, suggesting an extended application of OMVs when combined with the SpyTag/SpyCatcher system (44).

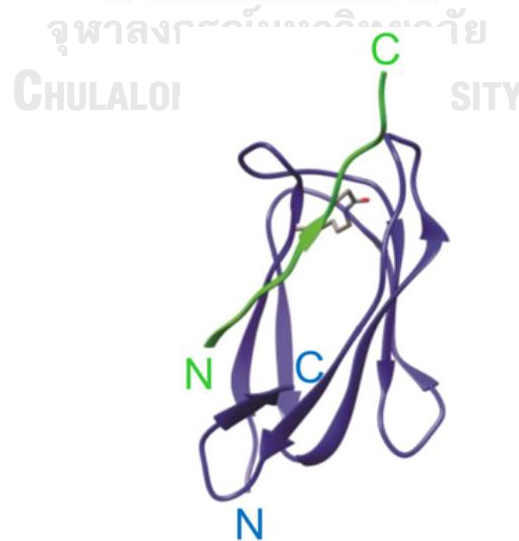


Figure 5 Ribbon structure of SpyTag/SpyCatcher. SpyTag is labelled in green and SpyCatcher is shown in blue. (Modified from (18))

4. Mucin 1

4.1. General information of mucin 1

Mucins are a family of transmembrane proteins expressed by epithelial cells found in various tissues such as intestinal tract, liver, pancreas, glandular, and lung. The unique structure of mucins is highlighted by hyper-glycosylation from most of O-linked glycans which contributes up to 90% of their molecular weight (64). As determined by their location, mucin members were classified into two types including secreted mucins (MUC2, MUC5AC, MUC5B, MUC6, and MUC7) and membrane-associated mucins (MUC1, MUC3, MUC4, MUC12, MUC13, MUC16, and MUC17) (22). Biological functions of mucins are thought to be involved in construction of epithelial barrier which aids protection of epithelial cells and cell-cell interaction (22, 23, 64). To be specific, secreted mucins like MUC2 could be exported to extracellular matrix and form gel-like layer which can limit bacterial infection, inflammation, and intense environment (65, 66). Not only secreted mucins but transmembrane mucins such as MUC1 and MUC4 also promote the mucinous layer by releasing their proteolytic products containing glycosylated moieties that can increase density of mucin-forming gel (23).

Mucin 1 (MUC1), alternately named as episialin, H23Ag, MCA, CD227, is a type I transmembrane mucin found abundantly in various epitheliums such as esophagus, stomach, lung, pancreas, mammary gland, and so on (22, 23, 64). In contrast to secreted mucins, MUC1 is anchored on the surface of the cell and poses a branch of O-linked glycosylated products which can elongate its extracellular domain to 200 – 500 nm beyond the cell membrane (67, 68). Generally, mature MUC1 is built as a heterodimer complex consisting of surface-exposed N-terminal subunit (MUC1-N) and short C-terminal cytoplasmic tail (MUC1-C) joined by hydrogen bonds (68, 69). The large fragment is composed of the signal peptide, the variable number tandem repeat (VNTR) region, and the Sea urchin sperm protein enterokinase and agrin (SEA) domain flanked by the imperfect repeat (IR). In the VNTR region, it is made of 20 – 120 repeats of 20 – 21 amino acids consisting of the glycan amino acid carriers like threonine and serine resulting in heavy O-linked glycosylation (70). The SEA domain was located next to GSVVV motif which is proteolytic cleavage site that allows automatically

splitting of two domains of MUC1 from a single encoded polypeptide after protein translation (67, 68). Unlike MUC1-N fragment, C-terminal domain of MUC1 is less complex and located in the cell membrane. The MUC1-C is included in the extracellular domain (ECD), transmembrane domain (TMD), and cytoplasmic tail (CT). Purposed functions of MUC1 are described by several studies including providing protection via mucin-forming gel and acting as a double-sword mediator in cell-cell and cell-matrix interactions (22, 23, 64). Specifically, bulky and extended structure of MUC1 may compromise intercellular interactions, while MUC1 from some tissue could act as adhesive molecules to present specified glycans to their receptor from other cells (71-74). In other respects, MUC1 also plays a role in signal transduction. For example, MUC1 could differ mitogen-activated protein kinase (MAPK) signaling cascades after phosphorylation of cytoplasmic domain (22). Likewise, cell proliferation and differentiation could be enhanced by activation of MUC1 since β -caterin could bind to C-terminus tail of MUC1 and transport it into nucleus resulting in activation of transcription processes of downstream products under transcriptional activator of β -caterin (75).

4.2. Relationship between MUC1 and cancer

As illustrated in figure 6, tumor-associated MUC1 is recognized by unique characteristics including 1) an aberrant expression of MUC1 which is observed by MUC1-overexpressing tumors from 900,000 per 1.4 million samples (23), 2) Redistribution of MUC1 polarity (76) and 3) Altered glycosylated modification (27, 77, 78). Alteration of glycosylated patterns in tumor-associated MUC1 is consisting of hypo-glycosylation and hyper-sialylation (79, 80). Unlike normal epithelial cells which express MUC1 with the Core 2 O-glycans, MUC1 from breast cancer presents the Core 1 O-glycans due to lack of glycosylation-related enzyme (81). Besides, truncated glycans produced from sialylations were found in abnormal MUC1 such as the sialylated Core 1 glycan found in breast cancer cells (82). As observed in colon cancer cells, other alternate glycans were found such as the sialyl LewisX (sLe^x) and sialyl Lewisia (sLe^a), suggesting the unique glycosylated decorations of MUC1 in tumor cells (83). Roles of MUC1 in cancers are involved in proliferation, invasion, and metastasis by using several mechanisms (22, 23, 64). For instance, similar to epithelial cells,

MUC1 from tumor cells could provide a protective barrier to avoid exposure of unfavorable environments and to control the microenvironment that drives invasive and metastatic tumor growth (22, 23, 79). Tumor-associated MUC1 could regulate glucose metabolism in cancer cells by modulating hypoxia-inducible factor-1 α (HIF-1 α) resulting in proliferation of cancer cells. Aside from HIF-1 α , MUC1 was evidenced to increase glucose uptake by mediating other related proteins as found in pancreas cancer cells, indicating complex functions of MUC1 in tumor progression (84).

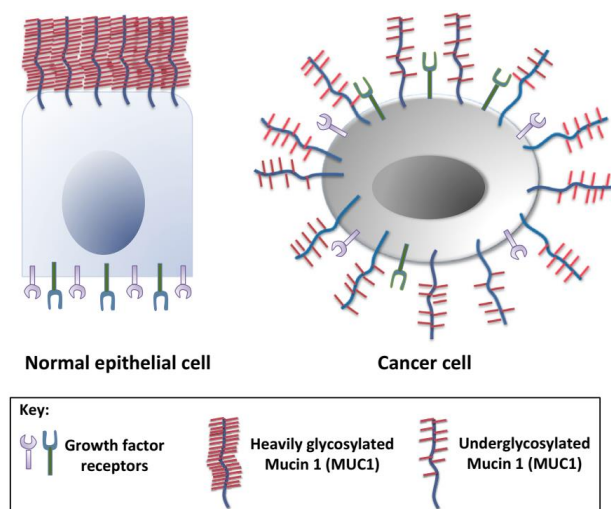


Figure 6 The structure of Mucin 1 in normal epithelial cells and tumor cells(85)

4.3. MUC1 as a promising target for cancer biomarker and treatment

The unique aberrant characteristics of tumor-associated MUC1 emphasize utilization of this protein in diagnosis and treatment. For example, due to the fact that MUC1-N fragment is found elevated in the serum of patients with breast cancer, the MUC1 (CA15-3) serum assay which detects the level of MUC1-N subunit is used to monitor breast cancer progression and treatment outcome and has been approved by U.S. FDA (86). Utilized by immunotherapy approaches, MUC1-based vaccines have been developed and currently under clinical phase. The types of a vaccine targeting MUC1 are consisting of subunit vaccine, viral vector vaccine, dendritic cell vaccine, and glycopeptide vaccine (87). The L-BLP25, a liposomal-based vaccine containing 25-residue of VNTR peptide, showed the safety and a promising outcome in clinical trial phase I and III as evaluated by an improved survival time after chemical treatments in patients with non-small lung cancer and prostate cancer (88, 89). However, combined

with clinical trial phase II result that is investigation of the efficacy of using L-BLP25 in colorectal cancer, the outcomes were not consistent in each subject. These findings indicate poor immunogenicity of this peptide-based MUC1 vaccine and require further improvement (90, 91). Apart from that, another strategy is to develop monoclonal antibodies to target epitopes on MUC1. The established antibodies are comprised of C595, HMFG1, BrE-3, SM3, and so on (92). Some of them have entered clinical trials and gave a promising outcome in various cancer types (93, 94). To give an example, the HMFG1 which recognizes hyperglycosylated VNTR core epitope (PDTR) could exhibit lower level of circulating MUC1 when patients were administrated by yttrium⁹⁰-labelled HMFG1 and treated subjects showed higher survival rate, suggesting a successful use of anti-MUC1 monoclonal antibody as an antibody-conjugated drug strategy (95). Moreover, recent study provided a concept of using antibody that binds to other epitopes than extracellular MUC1 epitopes. To illustrate, Min Jung Kim and team illustrated that the single-chain variable fragment targeting MUC1-C generated from a phage display process could reduce tumor invasion of triple-negative breast cancer cells, suggesting targeting MUC1 using alternative epitopes (96).

The SM3 antibody which recognizes glycan-nude VNTR core epitope (APDTRP) was derived from chemically-deglycosylated MUC1 from milk discovered by Joy Burchell and team (27). With high reactivity across various cancer types, it has been shown that SM3 could stain a variety of primary carcinomas including breast, colon, lung, and ovary (97). Owing to binding to hyperglycosylated epitope, SM3 showed weak interaction towards non-cancerous tissue that presents normal hyperglycosylated MUC1 (27, 97). Apart from using mature antibody, a single-chain variable fragment format was generated and derived from the parental sequence of intact SM3 antibody. This scFv SM3 was subsequently expressed on a nonreplicated live vector to prime macrophage to recognize MUC1. The results showed that an activated macrophage could eradicate MUC1-expressing tumor cells, but no effect in cells that do not have MUC1 (98). The use of scFv SM3 has been applied to development of a chimeric antigen receptor (CAR) T cell to aim immune-associated responses against MUC1-presenting cancer cells (99). Interestingly, Fengtao You and team improved binding capability of scFv SM3 via protein mutation and constructed it

into engineered CAR T cell. As conducted in clinical phase I, SM3-presenting CAR T cell elicited no severe side effects and could induce tumor necrosis in the patient with an advanced left seminal vesicle cancer (100). Because of these observations, it draws an attention to using SM3 in MUC1-assoicated cancer treatment.

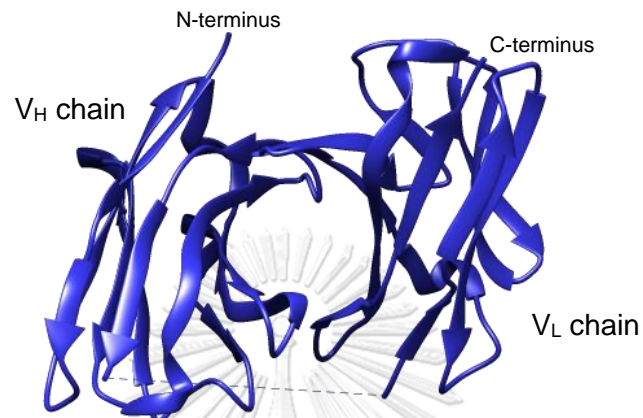


Figure 7 Three-dimensional structure of anti-MUC1 scFv clone SM3 consisting of V_H and V_L fragment linked by a flexible linker shown in a dash line (PDB ID: 5A2K)

CHAPTER III

MATERIALS AND METHODS

1) Chemicals

1.1) Cloning

Product	Supplier
Agarose (Molecular biology grade)	Vivantis, Malaysia
dNTP Set	Vivantis, Malaysia
RedSafe™ nucleic acid staining solution	iNtRON Biotechnology, Korea
PCR primers including T7 promoter, T7 terminator, 5LTR, and SV40	U2Bio, Thailand

1.2) Bacterial cultivation

Product	Supplier
Ampicillin sodium salt	Sigma-aldrich, USA
CRITERION™ LB agar	Hardy Diagnostics, USA
CRITERION™ LB broth Lennox	Hardy Diagnostics, USA
CRITERION™ LB broth Miller	Hardy Diagnostics, USA
Glycerol	Vivantis, Malaysia
OmniPur® IPTG	Merck, Germany
Tryptone	TM Media, India
Yeast extract	TM Media, India
Zeocin	Thermo Fisher Scientific, USA

1.3) Protein purification and biochemical analysis

Product	Supplier
Acrylamide/bis-acrylamide ready-to-use solution 30% (37.5:1)	Merck, Germany
Ammonium persulfate (APS)	Sigma-aldrich, USA
Bovine serum albumin (BSA)	Merck, Germany
Brilliant Blue R-250 (Coomassie Brilliant Blue R)	Merck, Germany
CRITERION™ skim milk powder	Hardy Diagnostics, USA
Glycine (NH ₂ ·CH ₂ COOH)	Bio-Rad Laboratories, USA
OmniPur® TEMED (Tetramethylethylenediamine)	Merck, Germany
Phenylmethylsulfonyl fluoride (PMSF)	PanReac Applichem, USA
Sodium dodecyl sulphate (SDS)	Bio-Rad Laboratories, USA
Triton™ X-100	Sigma-aldrich, USA
Tween®-20	Lobal Chemie, India

1.4) Chemicals for buffer preparation

Product	Supplier
Acetic acid	Qrac, Thailand
Imidazole for buffer solution	PanReac Applichem, USA
Paraformaldehyde	Sigma-aldrich, USA
Potassium chloride (KCl)	VWR International, USA
Potassium dihydrogen phosphate (KH ₂ PO ₄)	VWR International, USA
Propan-2-ol	RCI Labscan, Thailand
Sodium chloride (NaCl)	VWR International, USA
Sodium phosphate dibasic (Na ₂ HPO ₄)	VWR International, USA
Tris-hydroxymethyl aminomethane (Tris base)	Sigma-aldrich, USA
Tris-hydroxymethyl aminomethane HCl (Tris HCl)	SRL Chemical, India

1.5) Mammalian cell cultivation

Product	Supplier
Dulbecco's Modified Eagle Medium high glucose (DMEM)	Thermo Fisher Scientific, USA
Fetal Bovine Serum (FBS)	Thermo Fisher Scientific, USA
Penicillin-Streptomycin (10,000 U/ml)	Thermo Fisher Scientific, USA
Trypan blue solution (0.4%)	Thermo Fisher Scientific, USA
Trypsin-EDTA (0.25%, phenol red)	Thermo Fisher Scientific, USA

2) Cloning

2.1) Construction of plasmid encoding Lpp'OmpA-SpyCatcher for OMVs production

pLpp'OmpA-SpyCatcher was used to produce OMVs presenting Lpp'OmpA-SpyCatcher (OMVs:Lpp'OmpA-SpyCatcher) and is comprised of a gene encoding first nine amino acid of *lpp*, *ompA* gene (residue 46 – 159), *spycatcher* gene, C-terminal histidine-tag (HHHHHH), and interval GS-linker ((GSG)₂) (Complete sequence is available at figure 22 in appendix). This gene cassette (*lpp-ompA-spycatcher*) was flanked by NdeI cut site at 5' terminus and EcoRI cut site at 3' terminus and synthesized by Twist Bioscience, USA. The synthetic gene fragment and pET21a+ plasmid were digested by NdeI (New England Biolabs, UK) and EcoRI-HF (New England Biolabs, UK) as following protocol. Either 300 ng of synthetic gene fragment or 1500 ng of pET21a+ was mixed with 1 µl of 10X CutSmart™ Buffer, 0.3 µl of each NdeI and

EcoRI (6 units) and sterile water to a total reaction volume of 10 μ l. Then, the mixture was incubated at 37°C for 1 h. Digested products were purified by QIAquick PCR&Gel cleanup kit (QIAGEN, German) and the quality of purified DNA fragments was assessed by NanoDrop™ One/One® Microvolume UV-Vis Spectrophotometer (Thermo Fisher Scientific, USA). The purified DNA fragments were ligated using T4 DNA Ligase (New England Biolabs, UK) as following procedure. 50 μ g of digested pET21a+ was mixed to *lpp-ompa-spycatcher* purified gene fragment in a ratio of 1:5 mole ratio (calculated from <https://nebocalculator.neb.com>) together with 1 μ l of T4 DNA ligase buffer, 1 μ l of T4 DNA ligase (400 units), and sterile water to a total reaction volume of 10 μ l. The mixture was incubated at 16°C overnight and subsequently transformed to One Shot™ Mach1™ T1 Phage-Resistant Chemically Competent *E. coli* (Thermo Fisher Scientific, USA) using heat shock transformation method. Later, transformed bacteria were plated on LB agar plate supplemented with 100 μ g/ml ampicillin and incubated at 37°C overnight. Transformants that carry *lpp-ompa-spycatcher* in pET21a+ were selected by colony PCR. First, a single colony was resuspended in 15 μ l of lysis buffer (TE buffer plus 0.1% Triton™ X-100), heated at 95°C for 10 min, and centrifuged at 15,000 rpm for 10 min using Centrifuge 5430R (Eppendorf, Germany). Second, the supernatant was used as a template in PCR reaction using *Taq* DNA Polymerase, recombinant (Thermo Fisher Scientific, USA). The reaction of PCR reaction is consisting of 2 μ l of the supernatant, 1 μ l of 10X PCR buffer, 0.3 μ l of 50 mM MgCl₂, 0.2 μ l of 10 mM dNTP mix, 0.5 μ l of T7 promoter (5' TAATACGACTCACTATAGG 3'), 0.5 μ l of T7 terminator (5' GCTAGTTATTGCTCAGCGG 3'), 0.5 μ l of *Taq* DNA polymerase (2.5 units), and 5.45 μ l of sterile water. Thermocycler was performed using MiniAmp™ Plus Thermal Cycler (Thermo Fisher Scientific, USA) using following condition: 3 min of 94°C, 35 rounds of three steps (45 sec of 94°C, 30 sec of 55°C, 2 min 15 sec of 72°C), and 10 min of 72°C. Third, PCR products were analyzed by 1% agarose gel electrophoresis together with HyperLadder™ 1kb (Bioline, UK) using Sub-Cell® GT Agarose Gel Electrophoresis Systems (Bio-Rad Laboratories, USA) and PowerPac™ Basic Power Supply (Bio-Rad Laboratories, USA). Fourth, the gel was visualized by SafeViewer Blue Light Transilluminator (Hercuvan Lab System, UK). Clones that gave a positive

result (1,081 bp) were inoculated to LB broth supplemented with 100 µg/mL and shaken at 200 rpm 37°C for overnight using Refrigerated Shaking Incubator (Vertical type; N-BIOTEK, Korea). Next, the recombinant plasmid was purified from selected clones using Presto™ Mini Plasmid Kit (Geneaid, USA) and subjected to Sanger DNA sequencing (serviced by U2Bio, Thailand) for sequence verification.

2.2) Construction of plasmid for SpyTag-SM3 production

To express SpyTag-SM3, pSpyTag-SM3 was used and constructed in pFUSE-hIgG1-Fc2 (Invivogen, USA) backbone. The pSpyTag-SM3 has the organization of N-terminal histidine tag (HHHHHH), GS-linker ((GSG)₂), *spyttag* gene, GS-linker ((GSG)₂), codon-optimized anti-MUC1 scFv clone SM3 (98) (Complete sequence is available at figure 26 in appendix). This plasmid was made by replacement of *spyttag* gene to *spycatcher* gene in previously constructed plasmid (pSpyCatcher-SM3) containing N-terminal SpyCatcher fused to SM3 (Complete sequence is available at figure 25 in appendix). The *spycatcher* gene in pSpyCatcher-SM3 was depleted by sequential digestion of restriction enzymes that locate at 5' and 3' of *spycatcher* gene. 2000 ng of pSpyCatcher-SM3 was mixed with 0.5 µl of EcoRI-HF (10 units), 1 µl of 10X CutSmart™ Buffer and incubated at 37°C for 1 h. Then, the linearized plasmid was purified by QIAquick PCR&Gel cleanup kit followed by digestion using 0.5 µl of BglIII (10 units; New England Biolabs, UK) in a presence of 1X NEBuffer™ 3.1. The digestion mixture was incubated at 37°C for 1 h and analyzed on 1% agarose gel electrophoresis. The DNA band of *spycatcher*-depleted pSpyCatcher-SM3 (4,248 bp) was cut from the gel and purified by QIAquick PCR&Gel cleanup kit and observed DNA quality using NanoDrop™ One/One® Microvolume UV-Vis Spectrophotometer. The *spyttag* gene was inserted into *spycatcher*-depleted pSpyCatcher-SM3 by Gibson assembly technique. DNA fragment containing codon-optimized *spyttag* gene including 20 bp-overlapping *spycatcher*-depleted pSpyCatcher-SM3 sequence was synthesized by Twist Bioscience, USA. The assembly was performed by using NEBuilder® HiFi DNA Assembly master mix (New England Biolabs, UK) as following protocol. 0.033 pmol of *spycatcher*-depleted pSpyCatcher-SM3 and 0.167 pmol of *spyttag* gene fragment (calculated from <https://nebopcalculator.neb.com>) were incubated at 50°C for 1 h with 2.5 µl of NEBuilder® HiFi DNA Assembly Master Mix in a total reaction

volume of 5 μ l. Subsequently, One ShotTM Mach1TM T1 Phage-Resistant Chemically Competent *E. coli* was transformed by 2 μ l of reaction mixture using heat shock method. After incubation in LB (Lennox) agar supplemented with 25 μ g/mL of Zeocin at 37°C for overnight, transformants were selected by colony PCR as previously described in section 2.1 using 5LTR (5' TGCTTGCTCAACTCTACG 3') and SV40 (5' AACTTGTTTATTGCAGCTT 3') as PCR primers. PCR products were analyzed on 1% agarose gel electrophoresis. The clones that presented the positive result (1,169 bp) were cultured in LB broth (Lennox) supplemented with 25 μ g/mL of Zeocin at 200 rpm 37°C for overnight. Then, recombinant plasmids were purified by PrestoTM Mini Plasmid Kit and verified by Sanger DNA sequencing to ensure insert sequence.

3) Expression and isolation of OMVs:Lpp'OmpA-SpyCatcher

Expression and isolation of OMVs:Lpp'OmpA-SpyCatcher was performed as previous report with slight modifications (44). ECOS 21TM Competent Cells *E. coli* BL21(DE3) (YB Biotech, Taiwan) was transformed by pLpp'OmpA-SpyCatcher using heat shock method. The transformant was cultured in TB broth (2.4% tryptone, 1.2% yeast extract, 0.5% glycerol, and 89 mM phosphate buffer) supplemented with 100 μ g/ml ampicillin at 200 rpm 37°C for 16 – 18 h. The overnight culture was subsequently inoculated into fresh LB media and shaken at 200 rpm 37°C until OD₆₀₀ reached 0.6. The expression of Lpp'OmpA-SpyCatcher was induced by adding OmniPur[®] IPTG at a final concentration of 0.5 mM and the cells were allowed to grow at 200 rpm 30°C for 20 h. After that, intact bacteria and debris were removed by centrifugation of 7,000 rpm at 4°C for 30 min followed by filtration using Steritop Millipore Express PLUS 0.22 μ m (Merck, Germany). The OMVs-presenting supernatant was centrifuged at 150,000 x g 4°C for 3 h using Hitachi CP100NX Ultracentrifugation (Eppendorf Himac Technologies, Japan). The pellet was resuspended in 1/100 of initial volume using PBS and centrifuged at 15,000 rpm 4°C for 10 min. The purified OMVs was collected from supernatant, sterilized by 0.2 μ m Acrodisc[®] Syringe Filters 25 mm (Pall, China), and kept at -20°C until use. Total protein concentration of OMVs:Lpp'OmpA-SpyCatcher was determined by BCA assay using PierceTM BCA Protein Assay Kit (Thermo Fisher Scientific, USA).

4) Expression and purification of SpyTag-SM3

SpyTag-SM3 was aimed to be transiently expressed in ExpiCHO-S™ cells (Thermo Fisher Scientific, USA) using PEI MAX-mediated transfection method. Prior to perform mammalian expression processes, pSpyTag-SM3 was amplified by QIAGEN® Plasmid Maxi Kit (QIAGEN, German) and ExpiCHO-S™ cells were maintained in ExpiCHO™ expression medium (Thermo Fisher Scientific, USA) at humidified atmosphere of 8% CO₂ at 37°C and 125 rpm for at least three passages after thawing. A day before transfection, ExpiCHO-S™ cells were seeded at 0.5 x 10⁶ cells/mL in a total culture volume of 30 mL in Corning® 125 mL Polycarbonate Erlenmeyer Flask with Vent Cap (Corning, USA) and cultured for 24 h. At the day of transfection, 30 µg of pSpyTag-SM3 plasmid DNA and 90 µg of PEI MAX (MW 40,000; Polyscience, USA) were separately diluted in 1.5 mL of ExpiCHO™ expression medium and PEI MAX solution was subsequently dropped to plasmid DNA solution. After 10 min of incubation to create plasmid DNA-PEI MAX complex at room temperature, the complex was slowly transferred to cell suspension. After five days, the cells were removed by centrifugation of 5,000 x g 4°C for 30 min and the supernatant was clarified by filtration using 0.2 µm Acrodisc® Syringe Filters 25 mm. Next, SpyTag-SM3 was purified from the filtered supernatant using HisTrap FF 1 mL column (Cytiva, USA) equipped in ÄKTA Start (GE Healthcare Technologist, USA). The column was previously equilibrated with binding buffer (50 mM phosphate buffer, 300 mM NaCl, 20 mM Imidazole pH 8.0) and then loaded by the supernatant at a flow rate of 0.5 mL/min. After unbound proteins were washed by binding buffer for 10 column volume, SpyTag-SM3 was eluted by elution buffer (50 mM phosphate buffer, 300 mM NaCl, 250 mM Imidazole pH 8.0). SpyTag-SM3-containing fractions were pooled, buffer-exchanged to storage buffer (50 mM phosphate buffer, 150 mM NaCl pH 8.0), concentrated using Amicon® Ultra-4 centrifugal filter unit 10kDa cutoff (Merck, USA) and kept at -20°C until use. Protein concentration of SpyTag-SM3 was determined by BCA assay using Pierce™ BCA Protein Assay Kit.

5) SDS-PAGE and western blot

5.1) SDS-PAGE

The samples were prepared in 5X SDS-PAGE Protein Loading Buffer (Enzmart Biotech, Thailand) and heated at 95°C for 10 min. Then, the denatured samples were resolved on 10% SDS-polyacrylamide gel at 50 mA for 30 min using Mini-PROTEAN Tetra Cell (Bio-Rad Laboratories, USA) and PowerPac™ Basic Power Supply. The gel was stained by Coomassie Blue staining solution overnight and then de-stained by destaining solution until the gel was clear.

5.2) Western blot

After SDS-PAGE process, proteins in the gel were transferred to Immobilon-NC transfer membrane (Merck, USA) by Trans-Blot Semi-Dry Transfer Cell (Bio-Rad, USA) and PowerPac™ HC High-Current Power Supply (Bio-Rad, USA) using standard conditions (25 V and 30 min). Next, the membrane was briefly washed with TBST (Tris-buffer saline with 0.1% Tween-20) and blocked by 5% CRITERION™ Skim milk powder in TBST at room temperature for 2 h. The blot was probed by 1:20,000 diluted 6x-His Tag Monoclonal Antibody raised in mouse (HIS.H8; Thermo Fisher Scientific, USA) in 5% CRITERION™ Skim milk powder in TBST with gently rocking at room temperature for 60 min. After washing step of 3 times for 15 min interval, 1:200,000 diluted horseradish peroxidase (HRP)-conjugated anti-mouse IgG antibody (BioLegend, USA) in 5% CRITERION™ Skim milk powder in TBST was incubated with the membrane at room temperature for 30 min. The membrane was washed to remove excess antibodies. After that, HRP enzymatic reaction was carried out by adding Immobilon Forte Western HRP substrate (Merck, USA) for 3 min in dark place and immunological protein complexes were detected by using Chemiluminescent ImageQuant LAS4000 (Cytiva, USA).

6) Conjugation ratio optimization

As determined by BCA assay, OMVs:Lpp'OmpA-SpyCatcher and SpyTag-SM3 were mixed in a ratio of 1:0.2, 1:0.25, 1:0.33, 1:0.5, and 1:1 (weight-by-weight) as listed in table 2 and incubated at 4°C for 21 h. Conjugation reaction was quenched

by adding 5X SDS-PAGE Protein Loading Buffer and boiling. The samples were analyzed by using Western blot analysis as described in section 5.2. Intensity of conjugated product was quantified by Image J software (<https://imagej.nih.gov/ij/download.html>).

Table 2 Components of conjugated OMVs in various ratios

Conjugation ratio	OMVs:Lpp'OmpA-SpyCatcher (μg)	SpyTag-SM3 (μg)
1:0.2	7.5	1.50
1:0.25	7.5	1.88
1:0.33	7.5	2.50
1:0.5	7.5	3.75
1:1	7.5	7.5

7) Large-scale preparation of conjugated OMVs

SpyTag-SM3 was mixed with 2X weight excess of OMVs:Lpp'OmpA-SpyCatcher for 21 h at 4°C. Aggregations were removed by using 0.2 μm Acrodisc® Syringe Filters 25 mm and unreacted SpyTag-SM3 was removed by using Amicon® Ultra-4 centrifugal filter unit 100kDa cutoff (Merck, USA). The concentration of conjugated OMVs was determined by BCA assay using Pierce™ BCA Protein Assay Kit.

8) Dynamics light scattering

Size distribution profile of unconjugated OMVs (OMVs:Lpp'OmpA-SpyCatcher) and conjugated OMVs was observed by Zetasizer Nano ZS instrument (Malvern Panalytical, UK) using a standard protocol (Run duration = 60 s, number of runs = 5, number of measurements = 3). Both OMVs samples were prepared at a final concentration of 60 $\mu\text{g}/\text{mL}$ in 1 mL of PBS then loaded in a 12 mm square polystyrene cuvette. Data was collected by measuring 173° backscatter at 25°C. After that, the result was analyzed with Zetasizer Software (version 8.01).

9) Transmission electron microscopy

Morphology of the vesicles was observed by transmission electron microscopy (TEM) at Scientific Equipment and Research Division (SERD), Kasetsart University. In brief, 100 μl of 0.1 mg/mL of unconjugated OMVs and conjugated OMVs were

dropped on copper grids for 15 min. The copper grids were washed with water for a few times and blotted out by filter paper. Then, the vesicles were stained with 2% uranyl acetate for 30 s and observed by Hitachi HT7700 (Hitachi High-Technologies, USA) at 120 kV. An average diameter of OMVs samples were measured by Image J software (n=51).

10) Proteinase K protection assay

7 μg of conjugated OMVs was incubated in either a presence or an absence of 1% TritonTM X-100 on ice for 15 min followed by digestion by Proteinase K (Vivantis, Malaysia) at a final concentration of 0.1 mg/mL for 15 min at 37°C. Then, 10 μM of PMSF solution was added to stop proteolytic reaction and incubated on ice for 15 min. After that, the resulting samples were analyzed by SDS-PAGE and Western blot analysis as written in section 5.

11) Gold labelling TEM

Prior to perform conjugation reaction, SpyTag-SM3 was labelled by 10 nm gold nanoparticles at lysine residues using Gold Conjugation Kit (10 nm, 20 OD; Abcam UK) as manufacturer's protocol. 12 μl of 0.3 $\mu\text{g}/\text{mL}$ of SpyTag-SM3 was diluted in 42 μl reaction buffer. Then, 45 μl of mixture was used to dissolve lyophilized 10 nm gold nanoparticles by resting at room temperature for 15 min. The reaction was stopped by adding 5 μl of quencher buffer and then incubated for 5 min at room temperature. After that, 500 μl of 1:10 diluted quencher buffer was added and free SpyTag-SM3 was removed by centrifugation of 20,000 x g for 1 h at 4°C. Later, gold-labelled SpyTag-SM3 was resuspended from the pellet in a final volume of 50 μl using 1:10 diluted quencher buffer and kept in 4°C until use.

2 μg of OMVs:Lpp'OmpA-SpyCatcher was co-incubated with either 200 ng or 500 ng of gold-labelled SpyTag-SM3 in a total volume of 100 μl using PBS at 4°C for 21 h. Gold-labelled conjugated OMVs samples were subjected to TEM analysis as listed in section 9.

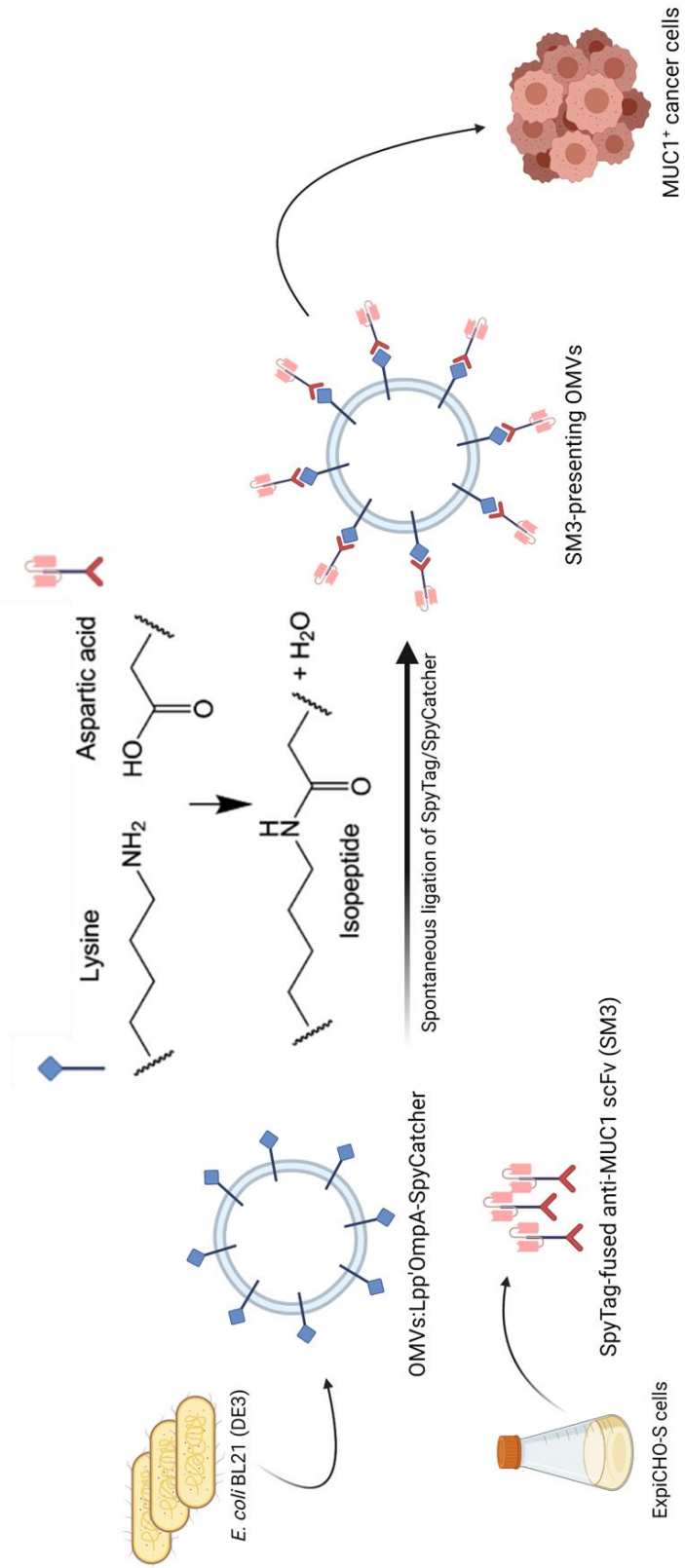
12) Cell-based ELISA (enzyme-linked immunosorbent assay)

MCF-7 (human breast cancer cell) kindly provided by Asst. Prof. Supannikar Tawinwung, Ph.D was maintained in DMEM supplemented with 10% of heat-inactivated FBS at humidified atmosphere of 5% CO₂ and 37°C. The cell was passaged when confluency reached around 70 - 80 % by enzymatic dissociation using 0.25% trypsin-EDTA and cultured at least three times post thawing before conducting an experiment.

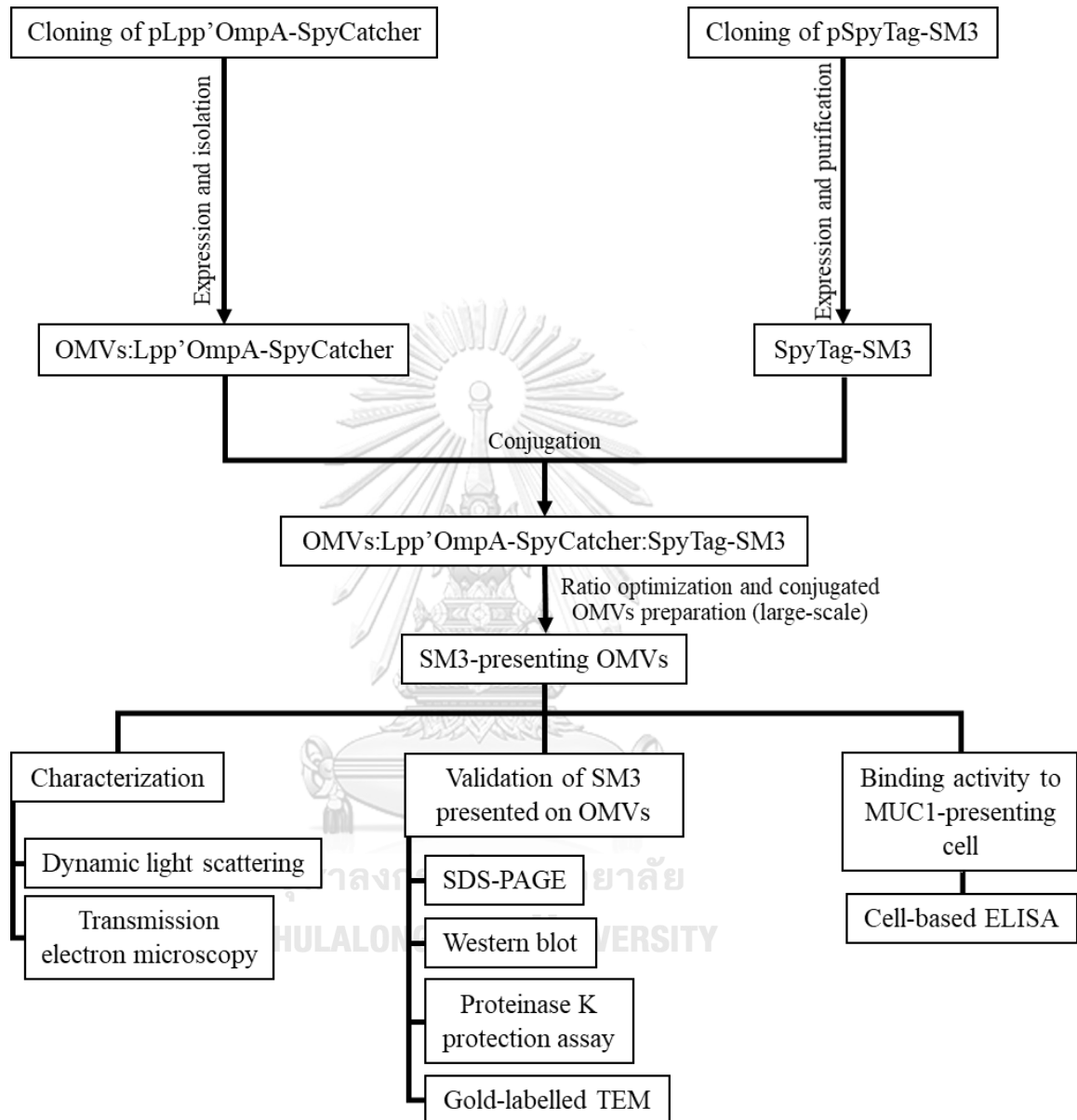
20,000 cells/well of MCF-7 was seeded into 96-well plate (Corning, USA) and allowed to grow for 24 h. Cells were washed with PBS twice and fixed by 100 µl of 4% paraformaldehyde in PBS for 20 min at room temperature. Then, the wells were washed with PBS twice and blocked with 200 µl of blocking buffer (5% BSA in PBS) for 2 h at 37°C. After washing with PBS, the cells were incubated with 10 µg of conjugated OMVs, 10 µg of unconjugated OMVs, 5 µg of purified SpyTag-SM3, or PBS serving as a negative control at 37°C for 1 h. Then, washing procedure was performed and 100 µl of 6x-His Tag Monoclonal Antibody raised in mouse (1:1000 diluted in blocking buffer) was added to the wells. After unbound antibodies were washed, 100 µl of HRP-conjugated anti-mouse IgG antibody (1:5000 diluted in blocking buffer) was added to the plate. Later, PBS was used to wash the plates and HRP reaction was initialized by 100 µl of TMB Chromogen Solution (for ELISA; Thermo Fisher Scientific, USA) for 15 min at room temperature. The reaction was stopped by an equal volume of 1N H₂SO₄ and colorimetric product was read at OD₄₅₀.

Statistical analysis of difference of mean between treated groups (conjugated OMVs, unconjugated OMVs and SpyTag-SM3) and negative control (PBS) was performed by GraphPad Prism version 9.2.0 using unpaired t-test.

Conceptual framework



Experimental design



CHAPTER IV

RESULTS

1. Construction of expression plasmids

In the present study, two expression plasmids were made consisting of pLpp'OmpA-SpyCatcher and pSpyTag-SM3 for production of *E. coli*-secreted OMVs anchoring Lpp'OmpA-SpyCatcher and recombinant SpyTag-SM3, respectively. The pLpp'OmpA-SpyCatcher was designed by cloning of *lpp'ompa-spycatcher* gene into pET-21a+ at NdeI/EcoRI recognition sites as shown in figure 8a. This pET-based vector allows high-level of protein production by IPTG-inducible T7 promoter to maximize Lpp'OmpA-SpyCatcher expression. The *lpp'ompa-spycatcher* gene cassette was added by gene encoding histidine-tag at C-terminus to ease detection of Lpp'OmpA-SpyCatcher expression. Each gene fragment was linked by a GS-linker ((GSG)₂) to retain their individual conformational structures and increase their flexibility of molecular movement (101). The pSpyTag-SM3 was constructed in pFUSE-hIgG1-Fc2 vector which is the mammalian expression plasmid containing secretory signal peptide (IL-2 sequence) to facilitate purification processes. This pFUSE-hIgG1-Fc2 employs elevated protein production via built-in promoter set including Elongation Factor-1 α (EF-1 α) core promoter and the R segment and part of the U5 sequence (R-U5') of the Human T-Cell Leukemia Virus (HTLV) Type 1 Long Terminal Repeat (5' LTR) (102, 103). As displayed in figure 8b, histidine-tag gene and was added after EcoRI recognition site resulting in N-terminal histidine-tagged protein expression which is frequently used in previous scFv production (33). Codon-optimized *spyttag* and the gene encoding heavy chain and light chain of scFv SM3 were constructed respectively and flanked by GS-linker.

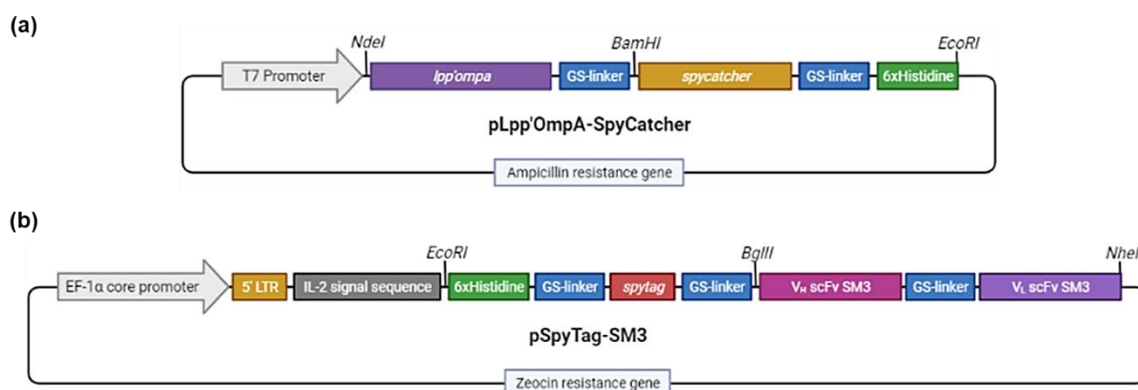


Figure 8 Schematic representation of expression plasmids used in this study . (a) Structure of pLpp'OmpA-SpyCatcher containing encoding gene of Lpp'OmpA (*lpp'ompA*) and SpyCatcher (*spycatcher*) and histidine-tag (6xHistidine). (b) Gene cassette encoding SpyTag-SM3 fusion protein constructed in pFUSE-hIgG1-Fc2 vector. Ampicillin and Zeocin resistance gene were included for bacterial selection in pLpp'OmpA-SpyCatcher and pSpyTag-SM3, respectively. The recognition sites of restriction enzyme were listed in italic in both gene maps. All schemes were created with BioRender.com.

Regarding the construction of pLpp'OmpA-SpyCatcher, a synthetic gene fragment of *lpp'ompA-spycatcher* plus histidine-tag gene was digested by *NdeI* and *EcoRI* and subsequently ligated into *NdeI/EcoRI*-digested pET21a+. The ligated product was transformed into *E. coli* strain Mach1TM. After that, transformants were firstly screened by colony PCR using T7 promoter and T7 terminator DNA sequences as primers. The agarose gel result revealed that 7 of 27 clones including clone number 3, 5, 10, 14, 16, 21, and 22 showed a positive PCR product of *lpp'ompA-spycatcher* at the size of 1,081 bp (figure 9). Then, plasmid from selected clones were verified by Sanger DNA sequencing. The sequencing results indicated identical DNA sequence of *lpp'ompA-spycatcher* gene cassette and recombinant plasmids from all selected clones except clone number 5 (figure 23 in appendix).

Cloning of pSpyTag-SM3 was carried out by replacement of *spytag* to *spycatcher* in previously made pSpyCatcher-SM3 using Gibson assembly technique. This seamless cloning method allows joining of DNA fragments in one reaction (104). A double-stranded DNA fragment containing *spytag* with 20-bp overlapping nucleotide

was ligated to *spycatcher*-depleted pSpyCatcher-SM3 using NEBuilder[®] HiFi DNA Assembly master mix. After that, transformants were plated on Zeocin-selective LB agar plate and afterwards analyzed by colony PCR using 5LTR and SV40 DNA sequences as primers. As shown in figure 10, there were 2 from 14 clones (clone number 12 and 13) that gave a positive PCR amplicon at 1,169 bp. Sequencing results of recombinant plasmids from both positive clones showed DNA sequence as designed (figure 27 in appendix).

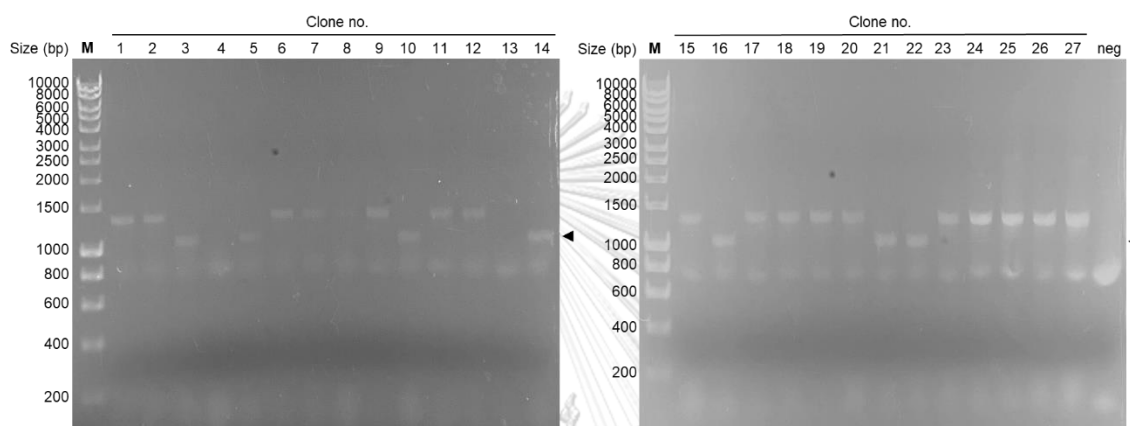


Figure 9 Colony PCR analysis of pLpp'OmpA-SpyCatcher transformants . Lane 1 – 27 represented PCR products from transformed clone number 1 to 27 while negative control was loaded at lane neg. HyperLadder[™] 1kb was shown in lane M. Arrows indicate positive PCR amplicon (1,081 bp).

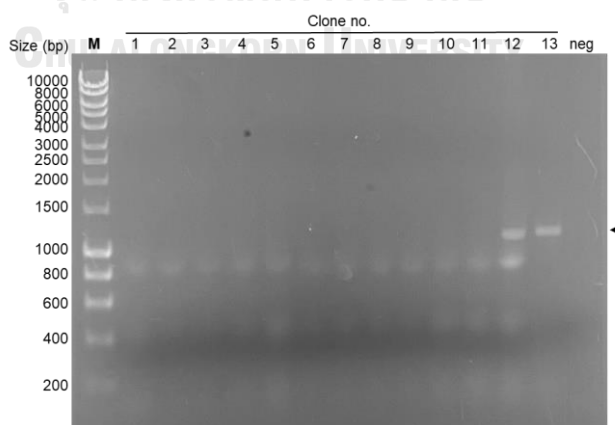


Figure 10 Colony PCR analysis of pSpyTag-SM3 from transformed clones. PCR products from clone number 1 to 13 were loaded in lane 1 – 13 together with negative

control at lane neg and HyperLadder™ 1kb at lane M. A black arrow points a positive PCR product (1,169 bp).

2. Isolation of *E. coli*-derived OMVs presenting Lpp'OmpA-SpyCatcher

The resulting pLpp'OmpA-SpyCatcher from clone 3 was subsequently transformed to *E. coli* strain BL21(DE3) which is compatible for T7 promoter-based vector and extensively used in OMVs production (44, 49, 56). After induction of Lpp'OmpA-SpyCatcher expression by IPTG, the cells were grown for 20 hours at 30°C. Removal of cells and debris was performed prior to pellet OMVs using ultracentrifugation. Then, purified OMVs presenting Lpp'OmpA-SpyCatcher (OMVs:Lpp'OmpA-SpyCatcher) was collected by additional centrifugation and further analyzed by SDS-PAGE and Western blot analysis. In figure 11a, it showed Coomassie-stained SDS-PAGE gel containing pre-induction and post-induction of cell lysates of pLpp'OmpA-SpyCatcher-transformed *E. coli* BL21(DE3) and purified OMVs. Due to massive protein contents in cell lysates and recombinant OMVs, we could not detect specific band of Lpp'OmpA-SpyCatcher from the Coomassie-stained gel. However, as evaluated by Western blotting using anti-histidine-tag antibody, an obvious band of Lpp'OmpA-SpyCatcher (29.9 kDa) was shown in the lane of post-induced whole cell lysate and purified OMVs (figure 11b). It suggested that the protein was expressed after IPTG induction and successfully localized in OMVs.

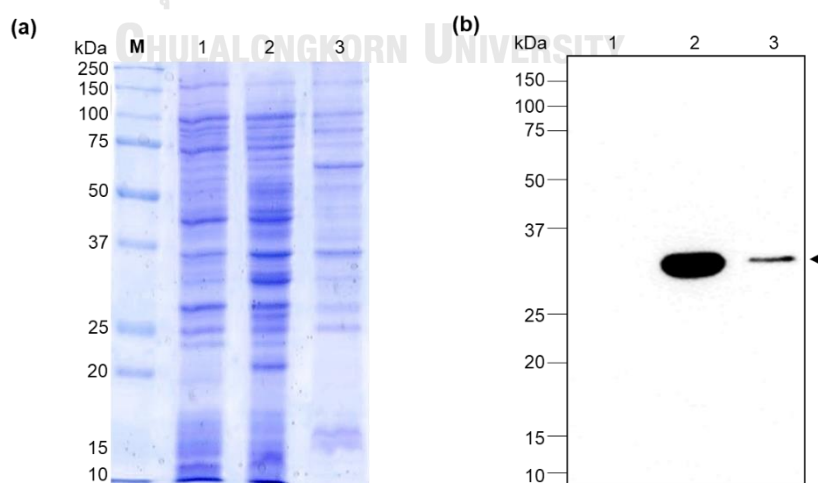


Figure 11 Expression and localization of Lpp'OmpA-SpyCatcher as determined by SDS-PAGE and Western blot. (a) Coomassie-stained SDS-PAGE gel containing pre-

induced and post-induced whole cell lysates (lane 1 and 2, respectively) and purified OMVs (lane 3). Precision Plus ProteinTM All Blue Prestained Protein Standards was presented at lane M. (b) Western blot analysis of cell lysates and OMVs using anti-histidine-tag antibody. An arrow indicates the protein band representing Lpp'OmpA-SpyCatcher.

3. Expression and purification of recombinant SpyTag-SM3

Unlike bacterial expression system, mammalian expression system provides disulfide linkage process which is required in recombinant scFv production to retain its structure and function (105, 106). As a result, we performed transient expression of SpyTag-fused scFv SM3 (SpyTag-SM3) in CHO-based system, ExpiCHO-STM cells. The pSpyTag-SM3 from clone 12 was transfected to ExpiCHO-STM cells by PEI MAX-mediated approach. After five days post transfection where cell viability was around 75%, cell-free supernatant containing recombinant SpyTag-SM3 was collected and subjected to purification via affinity column chromatography. The histidine-tagged SpyTag-SM3 was bound to Nickel Sepharose-prepacked column, HisTrap FF 1 mL column, and later eluted by imidazole-presenting elution buffer. The chromatogram from figure 12 illustrated that SpyTag-SM3 was successfully purified from host-cell contaminants after sudden change of elution buffer. After that, purified SpyTag-SM3 was examined by SDS-PAGE followed by Coomassie staining (figure 13a). The gel presented a distinct band at predicted size of SpyTag-SM3 (29.4 kDa). The fusion protein was also identified by immunoblotting using anti-histidine-tag antibody (figure 13b). The result is consistent with SDS-PAGE that a clear band representing SpyTag-SM3 was detected. These results indicated high homogeneity of purified SpyTag-SM3. Additionally, yield of SpyTag-SM3 production was achieved around 3 mg/L of culture.

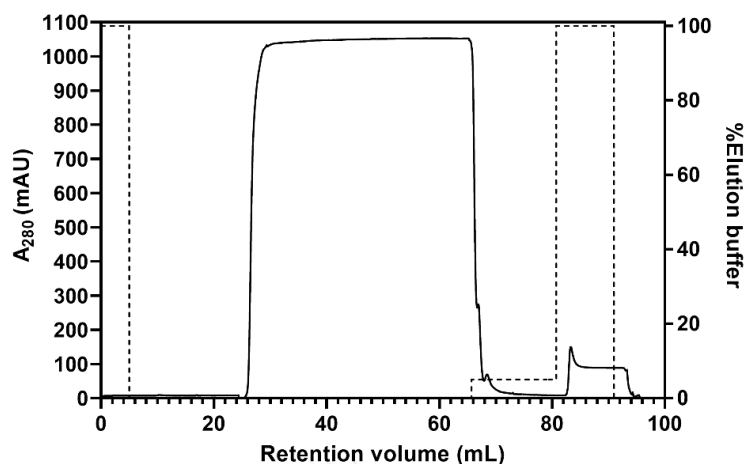


Figure 12 The chromatogram of SpyTag-SM3 purified from the supernatant of transfected cells by Nickel Sepharose-prepacked column. The column was previously equilibrated with the binding buffer (sodium phosphate buffer) and SpyTag-SM3 was eluted by the elution buffer (Imidazole-contained sodium phosphate buffer). Eluted profile was monitored at an absorbance of 280 nm and presented as a solid line. The percentage of elution buffer was shown in a dash line.

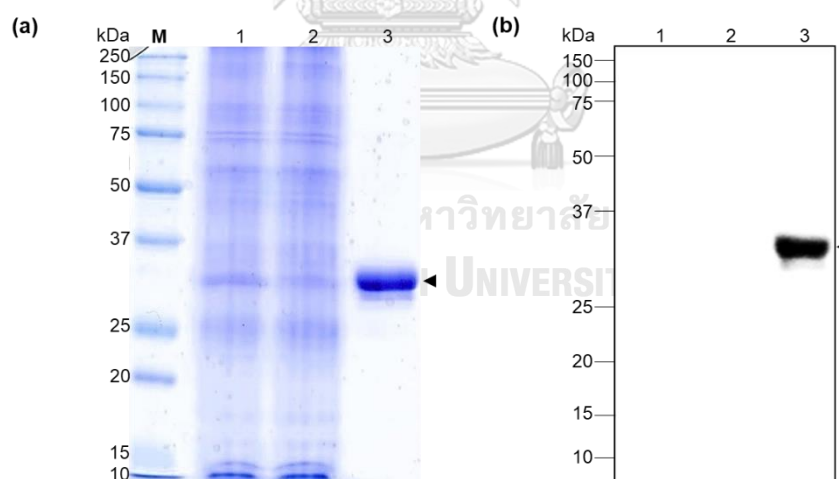


Figure 13 Identification of purified SpyTag-SM3 by SDS-PAGE analysis and Western blot . (a) Recombinant SpyTag-SM3 (lane 3) was analyzed by Coomassie-stained SDS-PAGE together with crude cell-free supernatant (lane 1) and flow-through fraction (lane 2). Precision Plus ProteinTM All Blue Prestained Protein Standards was loaded at lane M. (b) Validation of purified SpyTag-SM3 was carried out by Western blot analysis. Arrows show the protein band representing SpyTag-SM3 at ~29.4 kDa.

4. In vitro conjugation of OMVs:Lpp'OmpA-SpyCatcher and SpyTag-SM3

To couple SpyTag-SM3 with OMVs:Lpp'OmpA-SpyCatcher via SpyTag/SpyCatcher system, both components were mixed and incubated at 4°C for 21 hours as suggested by previous reports (18). Also, we optimized conjugation ratio by varying mass ratio (using protein concentration obtained from BCA assay) of OMVs:Lpp'OmpA-SpyCatcher and SpyTag-SM3 ranging from 1:0.2 to 1:1 to maximize SpyTag-SM3 attachment on the OMVs. Then, the conjugated product (Lpp'OmpA-SpyCatcher:SpyTag-SM3) from those ratios was examined by Western blot analysis using anti-histidine-tag antibody (figure 14a). The resulting blot displayed protein bands at 57.5 kDa which is relative to calculated size of the conjugated product. This calculated size is sum of Lpp'OmpA-SpyCatcher in size (29.9 kDa) and SpyTag-SM3 size (29.4 kDa) plus water removal upon SpyTag/SpyCatcher ligation chemistry. As collected from three independent experiments, conjugation products produced from those ratios were compared and indicated that the highest level of conjugated product could be achieved from conjugation ratio of 1:0.5 (figure 14b). At this ratio, the conjugation product was 1.6-fold higher than result from the conjugated product made by the ratio of 1:0.2. Besides, an average relative intensity of conjugated product from other ratios including 1:1, 1:0.33, and 1:0.25 were 1.48-, 1.51-, and 1.29-fold increase, respectively. Therefore, large-scale production of conjugated OMVs (SM3-presenting OMVs) was prepared by co-incubation of SpyTag-SM3 with 2-fold mass excess OMVs:Lpp'OmpA-SpyCatcher. After several washes of unreacted SpyTag-SM3 by 100 kDa cut-off ultrafiltration, conjugated product in the resulting OMVs was confirmed by Western blotting (figure 15).

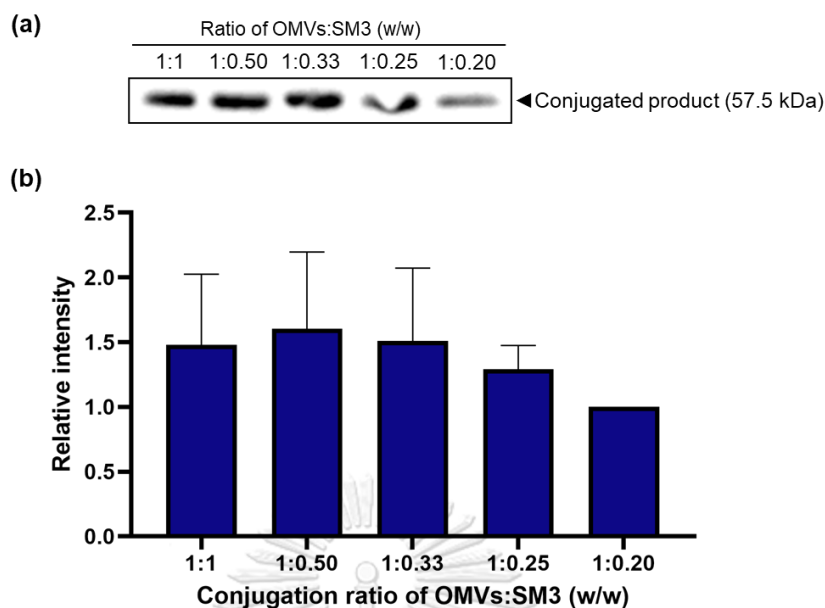


Figure 14 Optimization of conjugation ratio of OMVs:Lpp'OmpA-SpyCatcher and SpyTag-SM3 . (a) Conjugated products (Lpp'OmpA-SpyCatcher:SpyTag-SM3) from various conjugation ratio ranging from 1:0.2 to 1:1 (weight-by-weight ratio of OMVs:Lpp'OmpA-SpyCatcher and SpyTag-SM3) were visualized by Western blot analysis. (b) Intensity of conjugated products from Western blotting was quantified and normalized by the signal from ratio of 1:0.20. Data were collected from three independent experiments and represented as mean \pm SD.

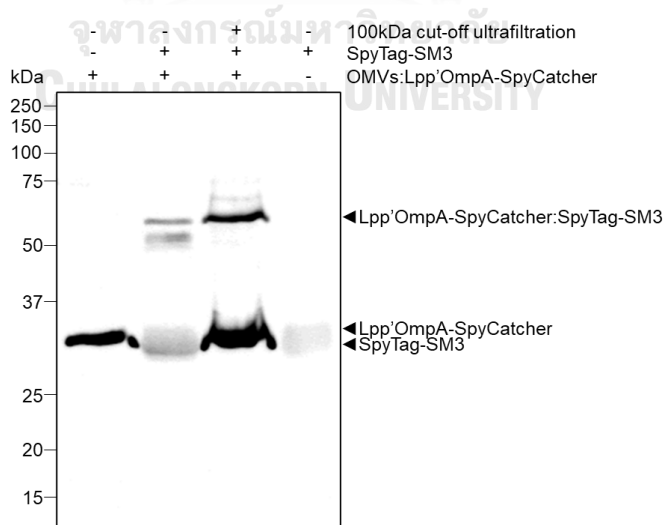


Figure 15 SpyTag/SpyCatcher ligation of SpyTag-SM3 to OMVs:Lpp'OmpA-SpyCatcher evaluated by immunoblotting analysis

5. Physiochemical characterizations of the vesicles

The OMVs samples including unconjugated OMVs and conjugated OMVs were characterized by dynamic light scattering (DLS) and transmission electron microscopy (TEM). As evaluated by DLS, the result revealed that an average hydrodynamic size of unconjugated OMVs was 97.42 nm and polydispersity index (PDI) was 0.278. Similar to the parental vesicle, conjugated OMVs had a hydrodynamic diameter of 103.7 nm and PDI of 0.287 suggesting that both OMVs are moderately polydisperse (figure 16). In addition, transmission electron microscopic images showed that both OMVs samples displayed spherical morphology with unique bilayer structure (figure 17). Notably, we did not observe significant changes in size and shape after conjugation, indicating that our conjugated OMVs still retained their physiochemical characteristics as unconjugated OMVs. Also, an averaged diameter of unconjugated OMVs and conjugated OMVs was revealed as 38.47 nm and 40.46 nm, respectively. The slight difference of vesicle sizes between unconjugated OMVs and conjugated OMVs is suggested to be affected by SpyTag-SM3 coated on the surface of OMVs.

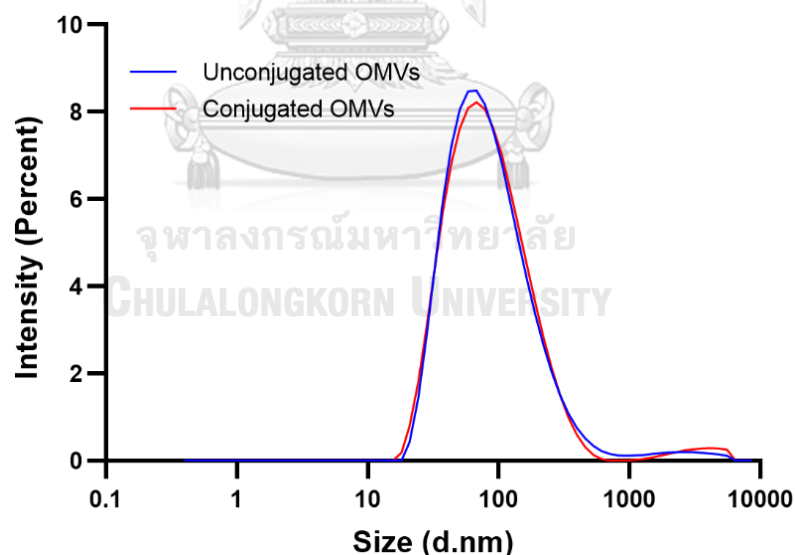


Figure 16 Size distribution profile of the vesicles determined by Dynamic light scattering including unconjugated OMVs (blue line) and conjugated OMVs (red line).

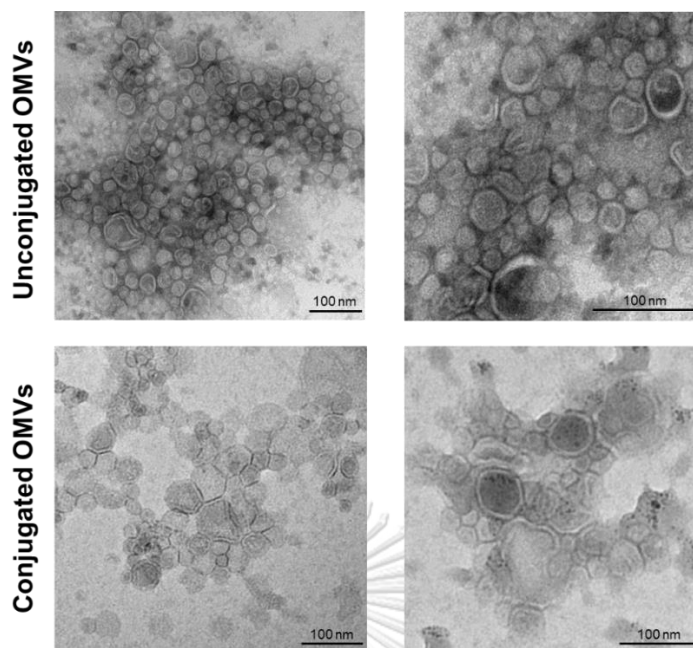


Figure 17 Transmission electron microscopic images of uranyl acetate-stained OMVs samples consisting of unconjugated OMVs (top row) and conjugated OMVs (bottom row). The bars indicate 100 nm.

6. Validation of scFv SM3 presentation on the surface of OMVs

As the conjugated OMVs will serve as a targeted drug delivery system to cancer cells, the position of SpyTag-SM3 must be exposed to the surface of OMVs. To confirm this, the location of scFv SM3 on the surface of OMVs was assessed by two methods including proteinase K protection assay and gold-labelled TEM. First, proteinase K protection assay utilizes detection of protease-susceptible proteins in extracellular space commonly used in OMVs-related studies (14, 45, 48, 54, 55). This method can distinguish location of proteins because only surface-exposed proteins could be digested by proteinase K in the absence of Triton X-100 (membrane destabilizer). On the contrary, both surface-exposed proteins and lumen-located proteins could be degraded by proteinase K in the presence of Triton X-100. We firstly ensure proteolytic activity of proteinase K by SDS-PAGE followed by Coomassie-blue staining (figure 18a). The gel showed decrease of protein bands after proteinase K treatment, suggesting an active enzymatic reaction of proteinase K. Since Lpp'OmpA-SpyCatcher and conjugated complex (Lpp'OmpA-SpyCatcher:SpyTag-SM3) could not be noticed by SDS-PAGE, we performed Western blot analysis to observe the proteinase-

susceptibility of those proteins. As displayed in figure 18b, degradation of conjugated complex was observed after proteinase K treatment without Triton X-100, indicating that SpyTag-SM3 was localized on the surface of OMVs. Remarkably, the protein band representing Lpp'OmpA-SpyCatcher was still remained after digestion by proteinase K without Triton X-100.

Second, gold-labelled TEM was performed by conjugation of OMVs:Lpp'OmpA-SpyCatcher and 10 nm gold nanoparticles-labelled SpyTag-SM3. Because of high electron density of gold nanoparticle, the gold nanoparticles gave dark spot when observed under TEM. This nature benefits us to detect presence of SpyTag-SM3 when conjugated to the OMVs. The gold-labelled TEM images showed dark spots resided on the membrane of conjugated OMVs while the background was clear of dark spots (figure 19). This result illustrated that SpyTag-SM3 could attach on the surface of the OMVs.

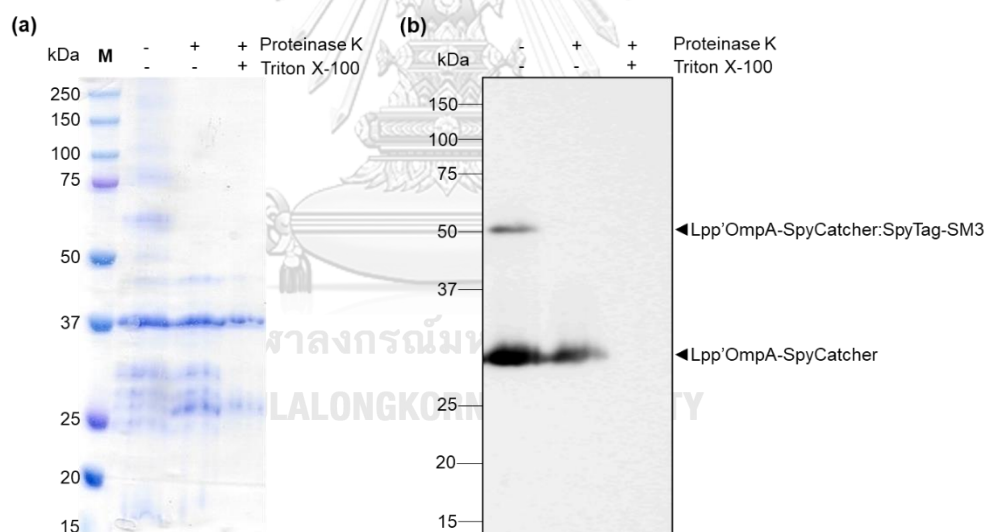


Figure 18 SDS-PAGE and Western blotting analysis presenting proteinase K protection assay of scFv SM3-presenting OMVs . The conjugated OMVs were digested by proteinase K with or without presence of Triton X-100. Non-treated conjugated OMVs served as a negative control.

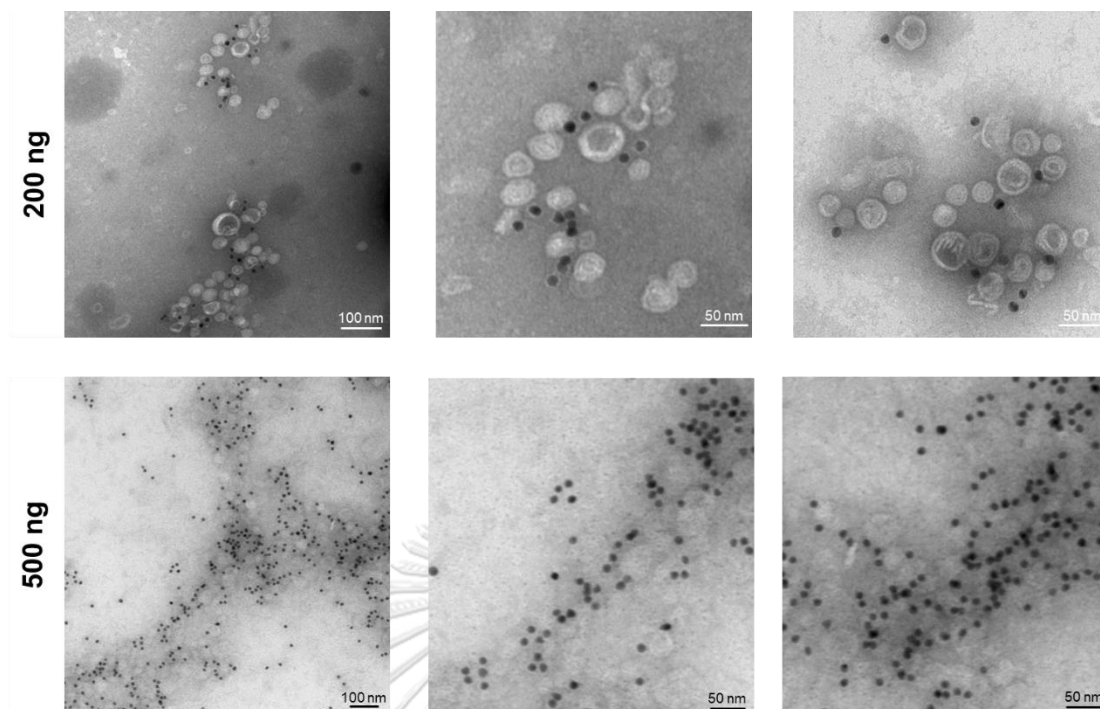


Figure 19 Gold-labelled TEM images . SpyTag-SM3 labeled by 10 nm gold nanoparticles was coupled to 2 μ g of OMVs:Lpp'OmpA-SpyCatcher and observed by TEM. Amount of gold-labelled SpyTag-SM3 (200 ng and 500 ng) was presented at the first column of each row. The dark spots indicate gold nanoparticles situated onto OMVs. The bars indicate individual scale in each image.

7. Binding analysis of scFv SM3-displaying OMVs to MUC1-presenting cell

To verify binding activity of scFv SM3-presenting OMVs to MUC1-expressing cell, we used MCF-7 cell as an *in vitro* model because it abundantly expresses MUC1 and previously used in MUC1-related studies (25, 96, 107). As shown in figure 20, the cell-based ELISA result showed that MCF-7 cells bound to purified SpyTag-SM3 could exhibit a significant signal compared to ones treated with PBS ($p < 0.05$). This suggested that SpyTag-SM3 could bind to MCF-7 cells. In addition, we observed a robust signal from binding with conjugated OMVs. This result demonstrated that scFv SM3 in conjugated OMVs retained binding activity to MCF-7 cells after conjugation to the OMVs via SpyTag/SpyCatcher system. However, a noticeable signal from unconjugated OMVs was also observed.

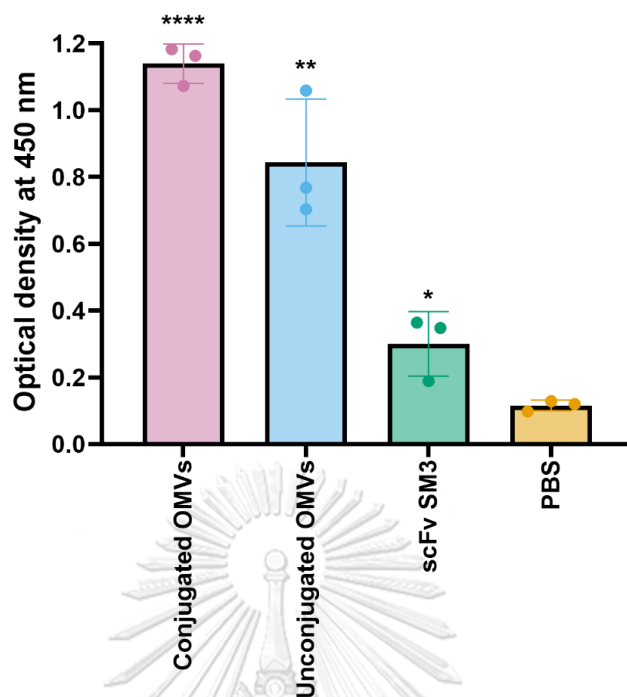


Figure 20 Binding activity of OMVs samples and scFv SM3 in MCF-7 cells evaluated by cell-based ELISA . The data is shown as mean of $OD_{450} \pm SD$ of three replicates. (*= $p < 0.05$; **= $p < 0.01$; ***= $p < 0.001$; ****= $p < 0.0001$)

CHAPTER V

DISCUSSION AND CONCLUSION

Bacterial OMVs gains wide attention recently due to their preferable advantages including stability, simple production, intrinsic adjuvanticity, and flexibility of modification. OMVs can serve as a vaccine platform as well as a multi-purpose delivery vehicle. Most studies from those applications were conducted in animal studies and some studies were performed in pre-clinical states supporting potential uses of OMVs in clinical applications (6, 8). In order to display heterologous proteins on OMVs, bacterial outer membrane-associated proteins such as ClyA and Hbp have been applied in bio-engineering of OMVs. These proteins can incorporate into bacterial outer membrane and export their fusion partner to OMVs in a surface-exposed manner. Apart from those carriers, we chose Lpp'OmpA as an alternative protein carrier because of its smaller size (~16 kDa) compared to the others (~34 kDa for ClyA and ~150 kDa for Hbp) (14, 15, 29). This benefit is expected to gain a higher density of Lpp'OmpA that anchors on an outer leaflet of OMVs leading to a higher presentation of target protein. In addition, even though ClyA has been served as a protein carrier in OMVs in many studies, it is still unknown whether undesirable effects from ClyA may be found. This is due to hemolytic activity so that it requires additional investigation to clarify toxicity of ClyA when used as a protein carrier in OMVs (14, 51). Furthermore, combined Lpp'OmpA system with SpyTag/SpyCatcher system, the boundary of OMVs display system which was previously restricted to present bacterial-produced proteins will be extended. As a result, we herein demonstrated a successful presentation of functional anti-MUC1 scFv produced from CHO cells on the surface of *E. coli*-derived OMVs via Lpp'OmpA plus SpyTag/SpyCatcher system to achieve MUC1-targeting OMVs utilized as a cell-specific drug vehicle.

As an attempt to obtain purified OMVs, several approaches have been used such as density gradient separation, precipitation, ultrafiltration, size-exclusion chromatography, and sequential centrifugations (34). In this study, we chose ultracentrifugation method to harvest crude OMVs because of its elevated benefits including less time-consuming and ease of procedure. The results revealed that the

pellet from ultracentrifugation contained OMVs:Lpp'OmpA-SpyCatcher as determined by SDS-PAGE and Western blot (figure 11) and TEM (figure 17) indicating successful OMVs isolation. Even though the previous report illustrated that overexpression of Lpp'OmpA fusion under a leaky promoter in high copy plasmid may affect bacterial membrane structure, we showed that our bioengineered OMVs still retained their original morphology (108, 109). It is consistent with the report from Nathan J. Alves et al. that OMVs expressing histidine-tag via Lpp'OmpA fusion were purified and showed no obvious changes of their structure (49). We suggested that altering bacterial membrane integrity from overexpressed Lpp'OmpA fusion may not affect the resulting OMVs structure. However, an amount of Lpp'OmpA-SpyCatcher in OMVs was suboptimal. As determined by the protease-accessibility assay, the blotting result illustrated that the remaining Lpp'OmpA-SpyCatcher was detected after proteinase K treatment without Triton X-100, implying that most of Lpp'OmpA residues was unable to integrate into the outer membrane and remained in the lumen of OMVs (figure 18). This phenomenon could be explained by inappropriate cultivation conditions which can be optimized to increase the number of Lpp'OmpA-SpyCatcher located in the outer membrane of OMVs such as cultivation time, media, and IPTG concentration.

Various targeting molecules such as affibody, nanobody, and scFv have been successfully incorporated into bioengineered OMVs to guide OMVs to the specific cells (54). In this study, a strategy to target MUC1-presenting cells was accomplished by using anti-MUC1 monoclonal antibody clone SM3 which binds to APDTRP at core epitope in variable number tandem repeat (VNTR) region of MUC1 (27, 92). Previously, intact anti-MUC1 antibody SM3 was able to distinguish cancer cells that express MUC1 and normal cells (27, 28, 92). In contrast to decorate OMVs with anti-MUC1 antibody SM3 as a mature form, we primarily engineered it as an scFv form because of its small size that aids purification processes and less bulkiness which may reduce steric interactions from an environment of outer membrane constituents leading to hindered SpyTag/SpyCatcher ligation efficacy. Utilized by CHO-based system, SpyTag-SM3 was successfully expressed and secreted in cell-free supernatant and subsequently purified by HisTrap column (figure 12). As predicted, the binding activity

of recombinant SpyTag-SM3 to MUC1 was confirmed by MCF-7 coated ELISA and the result showed that SpyTag-SM3 could bind to MCF-7, suggesting that purified recombinant SpyTag-SM3 could retain its binding functionality (figure 20). After coupling to OMVs:Lpp'OmpA-SpyCatcher, SpyTag-SM3 could be attached on the surface of the OMVs via SpyTag/SpyCatcher chemistry as illustrated in figure 15 and 19. Despite successful ligation, little amount of unreacted Lpp'OmpA-SpyCatcher was detected after performing the SpyTag/SpyCatcher ligation as indicated by a slight change of Lpp'OmpA-SpyCatcher intensity between proteinase K treated sample and non-digested sample (figure 18). This observation where one of SpyTag/SpyCatcher components was left after ligation was also found in another study (110). We assumed that crowded surface of the nanoparticles may affect the ligation efficacy of SpyTag and SpyCatcher. Next, we confirmed activity of binding to MCF-7 by anti-MUC1 scFv SM3 displayed on the OMVs by detection of an apparent signal from conjugated OMVs determined by cell-based ELISA (figure 20), this result encourages our bioengineered OMVs that display scFv SM3 as a promising MUC1-selective drug delivery system.

As the ultimate goal of this study is to generate functionalized cell-specific OMVs carrying drugs or therapeutic agents, our next step is to validate internalization of OMVs displaying scFv SM3 into MUC1-presenting cells to and thereby incorporate these agents into the OMVs serving as a cancer-targeted treatment. This utilization has been previously demonstrated by previous studies. For example, Vipul Gujrati and team showed that HER2-specific OMVs carrying a siRNA targeting kinesin spindle protein (KSP) could inhibit tumor growth affected by specific *ksp* gene silencing as evaluated by using *in vivo* model (10). A capability of OMVs to use in cancer treatment is supported by superior advantages such as 1) rigid structure and high stability which allows effective cargo delivery without massive leakage 2) small size of OMVs (20 – 200 nm) enables the enhanced permeability and retention (EPR) effect which benefits penetration and accumulation in tumor tissue (1, 10, 43). 3) immune responses that enhance anti-tumor activity through interactions of host immune cells and OMVs (1, 111).

While we showed encouraging results in this work, limitations of this study were also observed. First, the production of OMVs:Lpp'OmpA-SpyCatcher and

SpyTag-SM3 requires further optimization. As discussed earlier, cultivation conditions should be optimized to increase display of Lpp'OmpA-SpyCatcher in the surface of OMVs. Another attempt to increase protein density on the surface of OMVs is to produce OMVs in engineered *E. coli* strain. As illustrated by Ilaria Zanella et al., they removed a bunch of proteins that locate in OMVs resulting in an around 1.5-fold increase of heterologous protein loaded in OMVs (112). Moreover, yield of production of purified SpyTag-SM3 (3 mg/L) is lower than CHO-produced scFv yield from other studies (105, 106). Hence, expression conditions such as temperature, culture media, or establishing stable expression should be altered to reach optimal SpyTag-SM3 production yield. Second, it is needed to ensure that SM3 in unconjugated OMVs will not show binding to normal cells unless off-target effect could be found. This consideration could be validated by performing parallel analyses using MUC1-negative cell lines such as HCT-116, HEK293, HepG2, or MUC1-depleted MCF-7 generated by genome editing approach. Third, we observed that unconjugated OMVs omitted a significant binding signal towards MCF-7 cell indicating non-specific interaction of non-targeted OMVs. This phenomenon could be explained by non-specific interactions between OMVs and epithelial cells. It is also observed in previous studies that non-specific OMVs could internalize cancer cells (10, 43). However, this requires another investigation because that host cell-OMVs interactions are still unclear. Fourth, the detection strategy in cell-based ELISA is not appropriated to detect binding activity of conjugated OMVs. Due to histidine-tag that presented in both OMVs:Lpp'OmpA-SpyCatcher and SpyTag-SM3, the robust signal of conjugated OMVs is not directly related to binding of only scFv SM3 in conjugated OMVs to MCF-7 cells. Also, the signal elicited by non-specific binding of unconjugated OMVs could interfere actual signal from scFv SM3 as shown in an exceed signal from conjugated OMVs (figure 20). To overcome this issue, protein A could be used as a detection molecule since it can specifically bind to V_H of scFv (113). Another approach is to replace histidine-tag in OMVs:Lpp'OmpA-SpyCatcher to other tags such as FLAG, Myc, and Strep-tag so that the signals could be obtained from only histidine-tagged scFv SM3 (114). These methods could be performed to avoid redundant signals from non-specific binding of unconjugated OMVs.

In conclusion, utilized by the bio-ligation system of SpyTag/SpyCatcher, we provided a novel versatile protein decoration system on the surface of *E. coli*-derived OMVs. As shown in this study, anti-MUC1 scFv SM3 produced from CHO cells could be presented on bioengineered OMVs and retained its binding activity to MUC1-expressing cells, which will be beneficial to serve as targeted OMVs-based cancer therapy.



REFERENCES

1. Jiang L, Schinkel M, van Essen M, Schiffelers RM. Bacterial membrane vesicles as promising vaccine candidates. *Eur J Pharm Biopharm.* 2019;145:1-6.
2. Kaparakis-Liaskos M, Ferrero RL. Immune modulation by bacterial outer membrane vesicles. *Nat Rev Immunol.* 2015;15(6):375-87.
3. Jan AT. Outer Membrane Vesicles (OMVs) of Gram-negative Bacteria: A Perspective Update. *Front Microbiol.* 2017;8:1053.
4. Schwechheimer C, Kuehn MJ. Outer-membrane vesicles from Gram-negative bacteria: biogenesis and functions. *Nat Rev Microbiol.* 2015;13(10):605-19.
5. Wang S, Gao J, Wang Z. Outer membrane vesicles for vaccination and targeted drug delivery. *Wiley Interdiscip Rev Nanomed Nanobiotechnol.* 2019;11(2):e1523.
6. Gerritzen MJH, Martens DE, Wijffels RH, van der Pol L, Stork M. Bioengineering bacterial outer membrane vesicles as vaccine platform. *Biotechnol Adv.* 2017;35(5):565-74.
7. Carter NJ. Multicomponent meningococcal serogroup B vaccine (4CMenB; Bexsero(R)): a review of its use in primary and booster vaccination. *BioDrugs.* 2013;27(3):263-74.
8. Li R, Liu Q. Engineered Bacterial Outer Membrane Vesicles as Multifunctional Delivery Platforms. *Frontiers in Materials.* 2020;7.
9. Tan K, Li R, Huang X, Liu Q. Outer Membrane Vesicles: Current Status and Future Direction of These Novel Vaccine Adjuvants. *Front Microbiol.* 2018;9:783.
10. Gujrati V, Kim S, Kim S-H, Min JJ, Choy HE, Kim SC, et al. Bioengineered Bacterial Outer Membrane Vesicles as Cell-Specific Drug-Delivery Vehicles for Cancer Therapy. *ACS Nano.* 2014;8:1525-37.
11. Chen Q, Rozovsky S, Chen W. Engineering multi-functional bacterial outer membrane vesicles as modular nanodevices for biosensing and bioimaging. *Chem Commun (Camb).* 2017;53(54):7569-72.
12. Carvalho AL, Fonseca S, Miquel-Clopes A, Cross K, Kok KS, Wegmann U, et al. Bioengineering commensal bacteria-derived outer membrane vesicles for delivery of biologics to the gastrointestinal and respiratory tract. *J Extracell Vesicles.* 2019;8(1):1632100.
13. Gujrati V, Prakash J, Malekzadeh-Najafabadi J, Stiel A, Klemm U, Mettenleiter G, et al. Bioengineered bacterial vesicles as biological nano-heaters for optoacoustic imaging. *Nat Commun.* 2019;10(1):1114.
14. Kim JY, Doody AM, Chen DJ, Cremona GH, Shuler ML, Putnam D, et al. Engineered bacterial outer membrane vesicles with enhanced functionality. *J Mol Biol.* 2008;380(1):51-66.
15. Daleke-Schermerhorn MH, Felix T, Soprova Z, Ten Hagen-Jongman CM, Vikstrom D, Majlessi L, et al. Decoration of outer membrane vesicles with multiple antigens by using an autotransporter approach. *Appl Environ Microbiol.* 2014;80(18):5854-65.
16. Fantappie L, de Santis M, Chiarot E, Carboni F, Bensi G, Jousson O, et al. Antibody-mediated immunity induced by engineered *Escherichia coli* OMVs carrying heterologous antigens in their lumen. *J Extracell Vesicles.* 2014;3.

17. Zakeri B, Fierer JO, Celik E, Chittock EC, Schwarz-Linek U, Moy VT, et al. Peptide tag forming a rapid covalent bond to a protein, through engineering a bacterial adhesin. *Proc Natl Acad Sci U S A*. 2012;109(12):E690-7.
18. Keeble AH, Howarth M. Insider information on successful covalent protein coupling with help from SpyBank. *Methods Enzymol*. 2019;617:443-61.
19. Brune KD, Leneghan DB, Brian IJ, Ishizuka AS, Bachmann MF, Draper SJ, et al. Plug-and-Display: decoration of Virus-Like Particles via isopeptide bonds for modular immunization. *Scientific Reports*. 2016;6:1-13.
20. Lee S, Han BK, Kim YH, Ahn JY. SpyCatcher-SpyTagged ApxIA Toxoid and the Immune-Modulating Yeast Ghost Shells. *J Biomed Nanotechnol*. 2020;16(11):1644-57.
21. Li D, Zhang H, Yang L, Chen J, Zhang Y, Yu X, et al. Surface display of classical swine fever virus E2 glycoprotein on gram-positive enhancer matrix (GEM) particles via the SpyTag/SpyCatcher system. *Protein Expr Purif*. 2020;167:105526.
22. Hollingsworth MA, Swanson BJ. Mucins in cancer: protection and control of the cell surface. *Nat Rev Cancer*. 2004;4(1):45-60.
23. Kufe DW. Mucins in cancer: function, prognosis and therapy. *Nat Rev Cancer*. 2009;9(12):874-85.
24. Hamann PR, Hinman LM, Beyer CF, Lindh D, Upeslacijs J, Shochat D, et al. A Calicheamicin Conjugate with a Fully Humanized Anti-MUC1 Antibody Shows Potent Antitumor Effects in Breast and Ovarian Tumor Xenografts. *Bioconjugate Chemistry*. 2005;16:354-60.
25. Xu H, Gan L, Han Y, Da Y, Xiong J, Hong S, et al. Site-specific labeling of an anti-MUC1 antibody: probing the effects of conjugation and linker chemistry on the internalization process. *RSC Advances*. 2019;9(4):1909-17.
26. Taylor-Papadimitriou J, Peterson JA, Arklie J, Burchell J, Ceiuani RL, Bodmer WF. Monoclonal Antibodies to Epithelium-Specific Components of The Human Milk Fat Globule Membrane: Production and Reaction with Cells in Culture. *International Journal of Cancer*. 1981;28:17-21.
27. Burchell J, Gendler S, Taylor-Papadimitriou J, Girling A, Lewis A, Millis R, et al. Development and Characterization of Breast Cancer Reactive Monoclonal Antibodies Directed to the Core Protein of the Human Milk Mucin. *Cancer Research*. 1987;47:5476-82.
28. Posey AD, Jr., Clausen H, June CH. Distinguishing Truncated and Normal MUC1 Glycoform Targeting from Tn-MUC1-Specific CAR T Cells: Specificity Is the Key to Safety. *Immunity*. 2016;45(5):947-8.
29. Francisco JA, Earhart CF, Georgiou G. Transport and anchoring of β -lactamase to the external surface of *Escherichia coli*. *Proc Natl Acad Sci U S A*. 1992;89:2713-7.
30. Stathopoulos C, Georgiou G, Earhart CF. Characterization of *Escherichia coli* expressing an Lpp'OmpA(46-159)-PhoA fusion protein localized in the outer membrane. *Applied Microbiology and Biotechnology*. 1996;45:112-9.
31. Jo JH, Han CW, Kim SH, Kwon HJ, Lee HH. Surface display expression of *Bacillus licheniformis* lipase in *Escherichia coli* using Lpp'OmpA chimera. *J Microbiol*. 2014;52(10):856-62.
32. Huang S, Wei T, Sha W, Hu Q, Zhang Y, Wang J, et al. A simplified protein purification method through nickel cleavage of the recombinant protein from the *Escherichia coli* cell surface. *Analyst*. 2020;145(19):6227-31.

33. Ahmad ZA, Yeap SK, Ali AM, Ho WY, Alitheen NB, Hamid M. scFv antibody: principles and clinical application. *Clin Dev Immunol*. 2012;2012:980250.
34. Qing G, Gong N, Chen X, Chen J, Zhang H, Wang Y, et al. Natural and engineered bacterial outer membrane vesicles. *Biophysics Reports*. 2019;5(4):184-98.
35. Kulp A, Kuehn MJ. Biological functions and biogenesis of secreted bacterial outer membrane vesicles. *Annu Rev Microbiol*. 2010;64:163-84.
36. Kulkarni HM, Jagannadham MV. Biogenesis and multifaceted roles of outer membrane vesicles from Gram-negative bacteria. *Microbiology (Reading)*. 2014;160(Pt 10):2109-21.
37. Park JS, Lee WC, Yeo KJ, Ryu KS, Kumarasiri M, Heseck D, et al. Mechanism of anchoring of OmpA protein to the cell wall peptidoglycan of the gram-negative bacterial outer membrane. *FASEB J*. 2012;26(1):219-28.
38. Schertzer JW, Whiteley M. A bilayer-couple model of bacterial outer membrane vesicle biogenesis. *mBio*. 2012;3(2).
39. Haurat MF, Elhenawy W, Feldman MF. Prokaryotic membrane vesicles: new insights on biogenesis and biological roles. *Biol Chem*. 2015;396(2):95-109.
40. O'Donoghue EJ, Krachler AM. Mechanisms of outer membrane vesicle entry into host cells. *Cell Microbiol*. 2016;18(11):1508-17.
41. Lapinet JA, Scapini P, Calzetti F, Pérez O, Cassatella MA. Gene Expression and Production of Tumor Necrosis Factor Alpha, Interleukin-1b (IL-1b), IL-8, Macrophage Inflammatory Protein 1a (MIP-1a), MIP-1b, and Gamma Interferon-Inducible Protein 10 by Human Neutrophils Stimulated with Group B Meningococcal Outer Membrane Vesicles. *Infection and Immunity*. 2000;68: 6917–23.
42. Pulido MR, Garcia-Quintanilla M, Pachon J, McConnell MJ. A lipopolysaccharide-free outer membrane vesicle vaccine protects against *Acinetobacter baumannii* infection. *Vaccine*. 2020;38(4):719-24.
43. Kuerban K, Gao X, Zhang H, Liu J, Dong M, Wu L, et al. Doxorubicin-loaded bacterial outer-membrane vesicles exert enhanced anti-tumor efficacy in non-small-cell lung cancer. *Acta Pharm Sin B*. 2020;10(8):1534-48.
44. Alves NJ, Turner KB, Daniele MA, Oh E, Medintz IL, Walper SA. Bacterial Nanobioreactors--Directing Enzyme Packaging into Bacterial Outer Membrane Vesicles. *ACS Appl Mater Interfaces*. 2015;7(44):24963-72.
45. Huang W, Wang S, Yao Y, Xia Y, Yang X, Li K, et al. Employing *Escherichia coli*-derived outer membrane vesicles as an antigen delivery platform elicits protective immunity against *Acinetobacter baumannii* infection. *Scientific Reports*. 2016:1-12.
46. Kesty NC, Kuehn MJ. Incorporation of heterologous outer membrane and periplasmic proteins into *Escherichia coli* outer membrane vesicles. *J Biol Chem*. 2004;279(3):2069-76.
47. Basto AP, Piedade J, Ramalho R, Alves S, Soares H, Cornelis P, et al. A new cloning system based on the OprI lipoprotein for the production of recombinant bacterial cell wall-derived immunogenic formulations. *J Biotechnol*. 2012;157(1):50-63.
48. Bartolini E, Ianni E, Frigimelica E, Petracca R, Galli G, Berlanda Scorza F, et al. Recombinant outer membrane vesicles carrying *Chlamydia muridarum* HtrA induce antibodies that neutralize chlamydial infection in vitro. *J Extracell Vesicles*. 2013;2.
49. Alves NJ, Turner KB, DiVito KA, Daniele MA, Walper SA. Affinity purification of bacterial outer membrane vesicles (OMVs) utilizing a His-tag mutant. *Res Microbiol*. 2017;168(2):139-46.

50. Grandi A, Fantappie L, Irene C, Valensin S, Tomasi M, Stupia S, et al. Vaccination With a FAT1-Derived B Cell Epitope Combined With Tumor-Specific B and T Cell Epitopes Elicits Additive Protection in Cancer Mouse Models. *Front Oncol.* 2018;8:481.
51. Chen DJ, Osterrieder N, Metzger SM, Buckles E, Doody AM, DeLisa MP, et al. Delivery of foreign antigens by engineered outer membrane vesicle vaccines. *Proc Natl Acad Sci U S A.* 2010;107(7):3099-104.
52. Quan K, Zhu Z, Cao S, Zhang F, Miao C, Wen X, et al. Escherichia coli-Derived Outer Membrane Vesicles Deliver Galactose-1-Phosphate Uridyltransferase and Yield Partial Protection against Actinobacillus pleuropneumoniae in Mice. *J Microbiol Biotechnol.* 2018;28(12):2095-105.
53. Rappazzo CG, Watkins HC, Guarino CM, Chau A, Lopez JL, DeLisa MP, et al. Recombinant M2e outer membrane vesicle vaccines protect against lethal influenza A challenge in BALB/c mice. *Vaccine.* 2016;34(10):1252-8.
54. Saparoea HBvdBv, Houben D, Jonge MId, Jong WSP, Luirink J. Display of Recombinant Proteins on Bacterial Outer Membrane Vesicles by Using Protein Ligation. *Applied and Environmental Microbiology.* 2018;84(8):1-17.
55. van den Berg van Saparoea HB, Houben D, Kuijl C, Luirink J, Jong WSP. Combining Protein Ligation Systems to Expand the Functionality of Semi-Synthetic Outer Membrane Vesicle Nanoparticles. *Front Microbiol.* 2020;11:890.
56. Cheng K, Zhao R, Li Y, Qi Y, Wang Y, Zhang Y, et al. Bioengineered bacteria-derived outer membrane vesicles as a versatile antigen display platform for tumor vaccination via Plug-and-Display technology. *Nat Commun.* 2021;12(1):2041.
57. Cabrera-Valladares N, Martínez A, Piñero S, Lagunas-Muñoz VH, Tinoco R, de Anda R, et al. Expression of the melA gene from Rhizobium etli CFN42 in Escherichia coli and characterization of the encoded tyrosinase. *Enzyme and Microbial Technology.* 2006;38(6):772-9.
58. Ghrayeb J, Inouye M. Nine Amino Acid Residues at the NH₂-terminal of Lipoprotein Are Sufficient for Its Modification, Processing, and Localization in the Outer Membrane of *Escherichia coli*. *The Journal of Biological Chemistry.* 1984;259:463-7.
59. Yamaguchi K, Yu F, Inouye M. A Single Amino Acid Determinant of the Membrane Localization of Lipoproteins in *E. coli*. *Cell.* 1988;53:423-32.
60. S.Daugherty P, Chen G, J.Olsen M, L.Iverson B, Georgiou G. Antibody affinity maturation using bacterial surface display. *Protein Engineering.* 1998;11:825-32.
61. Hagen A, Sutter M, Sloan N, Kerfeld CA. Programmed loading and rapid purification of engineered bacterial microcompartment shells. *Nat Commun.* 2018;9(1):2881.
62. Pedroso CCS, Mann VR, Zuberbuhler K, Bohn MF, Yu J, Altoe V, et al. Immunotargeting of Nanocrystals by SpyCatcher Conjugation of Engineered Antibodies. *ACS Nano.* 2021.
63. Li L, Fierer JO, Rapoport TA, Howarth M. Structural analysis and optimization of the covalent association between SpyCatcher and a peptide Tag. *J Mol Biol.* 2014;426(2):309-17.
64. Gendler SJ. MUC1, The Renaissance Molecule. *Journal of Mammary Gland Biology and Neoplasia.* 2001;6:339-53.

65. Xavier RJ, Podolsky DK. Unravelling the pathogenesis of inflammatory bowel disease. *Nature*. 2007;448(7152):427-34.
66. Johansson MEV, Phillipson M, Petersson J, Velcich A, Holm L, Hansson GC. The inner of the two Muc2 mucin-dependent mucus layers in colon is devoid of bacteria. *Proc Natl Acad Sci U S A*. 2008;105:15064-9.
67. Gendler SJ, Spicer AP. Epithelial mucin genes. *Annu Rev Physiol*. 1995;57:607-34.
68. Hattstrup CL, Gendler SJ. Structure and function of the cell surface (tethered) mucins. *Annu Rev Physiol*. 2008;70:431-57.
69. Levitin F, Stern O, Weiss M, Gil-Henn C, Ziv R, Prokocimer Z, et al. The MUC1 SEA module is a self-cleaving domain. *J Biol Chem*. 2005;280(39):33374-86.
70. Creaney J, Segal A, Sterrett G, Platten MA, Baker E, Murch AR, et al. Overexpression and altered glycosylation of MUC1 in malignant mesothelioma. *Br J Cancer*. 2008;98(9):1562-9.
71. Ligtenberg MJ, Kruijshaar L, Buijs F, van Meijer M, Litvinov SV, Hilkens J. Cell-associated episialin is a complex containing two proteins derived from a common precursor. *Journal of Biological Chemistry*. 1992;267(9):6171-7.
72. Fontenot JD, Tjandra N, Bu D, Ho C, Montelaro RC, Finn OJ. Biophysical Characterization of One-, Two-, and Three-Tandem Repeats of Human Mucin (muc-1) Protein Core1. *Cancer Research*. 1993;53:5386-94.
73. Hanski C, Drechsler K, Hanisch F-G, Sheehan J, Manske M, Ogorek D, et al. Altered Glycosylation of the MUC-1 Protein Core Contributes to the Colon Carcinoma-associated Increase of Mucin-bound Sialyl-Lewis^x Expression. *Cancer Research*. 1993;4082-8.
74. Zhang K, Baeckstrom D, Brevinge H, Hansson CC. Secreted MUC1 Mucins Lacking Their Cytoplasmic Part and Carrying Sialyl-Lewis a and-x Epitopes From a Tumor Cell Line and Sera of Colon Carcinoma Patients Can Inhibit HL-60 Leukocyte Adhesion to E-Selectin-Expressing Endothelial Cells. *Journal of Cellular Biochemistry*. 1996;60:538-49.
75. Yamamoto M, Bharti A, Li Y, Kufe D. Interaction of the DF3/MUC1 breast carcinoma-associated antigen and beta-catenin in cell adhesion. *J Biol Chem*. 1997;272(19):12492-4.
76. Altschuler Y, Kinlough CL, Poland PA, Apodaca G, Weisz OA, Bruns JB, et al. Clathrin-mediated Endocytosis of MUC1 Is Modulated by Its Glycosylation State. *Molecular Biology of the Cell*. 2000;11:819-31.
77. Percy L, Hayes DF, Maimonis P, Abe M, O'Hara C, Kufe DW. Tumor Selective Reactivity of a Monoclonal Antibody Prepared against a Recombinant Peptide Derived from the DF3 Human Breast Carcinoma-associated Antigen. *Cancer Research*. 1992;2563-8.
78. Muller S, Alving K, Peter-Katalinic J, Zachara N, Gooley AA, Hanisch FG. High density O-glycosylation on tandem repeat peptide from secretory MUC1 of T47D breast cancer cells. *J Biol Chem*. 1999;274(26):18165-72.
79. Horm TM, Schroeder JA. MUC1 and metastatic cancer: expression, function and therapeutic targeting. *Cell Adh Migr*. 2013;7(2):187-98.
80. Corfield AP. Mucins: a biologically relevant glycan barrier in mucosal protection. *Biochim Biophys Acta*. 2015;1850(1):236-52.

81. Brockhausen I, Yang J-M, Burchell J, Whitehouse C, Taylor-Papadimitriou J. Mechanisms underlying aberrant glycosylation of MUC1 mucin in breast cancer cells. *Eur J Biochem.* 1995;233:607-17.
82. Picco G, Julien S, Brockhausen I, Beatson R, Antonopoulos A, Haslam S, et al. Over-expression of ST3Gal-I promotes mammary tumorigenesis. *Glycobiology.* 2010;20(10):1241-50.
83. Mann B, Klussmann E, Vandamme-Feldhaus V, Iwersen M, Hanski M-L, Riecken E-O, et al. Low O-Acetylation of Sialyl-Lex Contributes to Its Overexpression in Colon Carcinoma Metastases. *Int J Cancer.* 1997;72:258-64.
84. Chaika NV, Gebregiworgis T, Lewallen ME, Purohit V, Radhakrishnan P, Liu X, et al. MUC1 mucin stabilizes and activates hypoxia-inducible factor 1 alpha to regulate metabolism in pancreatic cancer. *Proc Natl Acad Sci U S A.* 2012;109(34):13787-92.
85. Nath S, Mukherjee P. MUC1: a multifaceted oncoprotein with a key role in cancer progression. *Trends Mol Med.* 2014;20(6):332-42.
86. Hayes DF, Sekine H, Ohno T, Abe M, Keefe K, Kufe DW. Use of a murine monoclonal antibody for detection of circulating plasma DF3 antigen levels in breast cancer patients. *J Clin Invest.* 1985;75(5):1671-8.
87. Gao T, Cen Q, Lei H. A review on development of MUC1-based cancer vaccine. *Biomed Pharmacother.* 2020;132:110888.
88. Palmer M, Parker J, Modi S, Butts C, Smylie M, Meikle A, et al. Phase I study of the BLP25 (MUC1 peptide) liposomal vaccine for active specific immunotherapy in stage IIIB/IV non-small-cell lung cancer. *Clin Lung Cancer.* 2001;3(1):49-57; discussion 8.
89. North SA, Graham K, Bodnar D, Venner P. A Pilot Study of the Liposomal MUC1 Vaccine BLP25 in Prostate Specific Antigen Failures After Radical Prostatectomy. *Journal of Urology.* 2006;176(1):91-5.
90. Schimanski CC, Mohler M, Schon M, van Cutsem E, Greil R, Bechstein WO, et al. LICC: L-BLP25 in patients with colorectal carcinoma after curative resection of hepatic metastases: a randomized, placebo-controlled, multicenter, multinational, double-blinded phase II trial. *BMC Cancer.* 2012;12:144.
91. Rivalland G, Loveland B, Mitchell P. Update on Mucin-1 immunotherapy in cancer: a clinical perspective. *Expert Opin Biol Ther.* 2015;15(12):1773-87.
92. Burke PA, Gregg JP, Bakhtiar B, Beckett LA, Denardo GL, Albrecht H, et al. Characterization of MUC1 glycoprotein on prostate cancer for selection of targeting molecules. *International Journal of Oncology.* 2006;29:49-55.
93. Hisatsune A, Nakayama H, Kawasaki M, Horie I, Miyata T, Isohama Y, et al. Anti-MUC1 antibody inhibits EGF receptor signaling in cancer cells. *Biochem Biophys Res Commun.* 2011;405(3):377-81.
94. Wang L, Chen H, Pourgholami MH, Beretov J, Hao J, Chao H, et al. Anti-MUC1 monoclonal antibody (C595) and docetaxel markedly reduce tumor burden and ascites, and prolong survival in an in vivo ovarian cancer model. *PLoS One.* 2011;6(9):e24405.
95. Oei AL, Moreno M, Verheijen RH, Sweep FC, Thomas CM, Massuger LF, et al. Induction of IgG antibodies to MUC1 and survival in patients with epithelial ovarian cancer. *Int J Cancer.* 2008;123(8):1848-53.

96. Kim MJ, Choi JR, Tae N, Wi TM, Kim KM, Kim DH, et al. Novel Antibodies Targeting MUC1-C Showed Anti-Metastasis and Growth-Inhibitory Effects on Human Breast Cancer Cells. *Int J Mol Sci.* 2020;21(9).
97. Girling A, Bartkova J, Burchell J, Gendler S, Gillett C, Taylor-Papadimitriou J. A Core Protein Epitope of The Polymorphic Epithelial Mucin Exposed in A Range of Primary Carcinomas Detected by The Monoclonal Antibody SM-3 Is Selectively. *Int J Cancer.* 1989;43:1072-6.
98. Paul S, Snary D, Hoebeke J, Allen D, Balloul J-M, Bizouarne N, et al. Targeted Macrophage Cytotoxicity Using a Nonreplicative Live Vector Expressing a Tumor-Specific Single-Chain Variable Region Fragment. *Human Gene Therapy.* 2000;11:1417-28.
99. Wilkie S, Picco G, Foster J, Davies DM, Julien S, Cooper L, et al. Retargeting of Human T Cells to Tumor-Associated MUC1: The Evolution of a Chimeric Antigen Receptor. *The Journal of Immunology.* 2008;180:4901-9.
100. You F, Jiang L, Zhang B, Lu Q, Zhou Q, Liao X, et al. Phase 1 clinical trial demonstrated that MUC1 positive metastatic seminal vesicle cancer can be effectively eradicated by modified Anti-MUC1 chimeric antigen receptor transduced T cells. *Sci China Life Sci.* 2016;59(4):386-97.
101. Chen X, Zaro JL, Shen WC. Fusion protein linkers: property, design and functionality. *Adv Drug Deliv Rev.* 2013;65(10):1357-69.
102. Takebe Y, Seiki M, Fujisawa J-I, Hoy P, Yokota K, Arai K-I, et al. SR α Promoter: an Efficient and Versatile Mammalian cDNA Expression System Composed of the Simian Virus 40 Early Promoter and the R-U5 Segment of Human T-Cell Leukemia Virus Type 1 Long Terminal Repeat. *Molecular and Cellular Biology.* 1988;8:466-72.
103. Kim DW, Uetsuki T, Kaziro Y, Yamaguchi N, Sugano S. Use of the human elongation factor 1 α promoter as a versatile and efficient expression system. *Gene.* 1990;91:217-23.
104. Gibson DG, Young L, Chuang RY, Venter JC, Hutchison CA, 3rd, Smith HO. Enzymatic assembly of DNA molecules up to several hundred kilobases. *Nat Methods.* 2009;6(5):343-5.
105. Zuberbuhler K, Palumbo A, Bacci C, Giovannoni L, Sommariva R, Kaspar M, et al. A general method for the selection of high-level scFv and IgG antibody expression by stably transfected mammalian cells. *Protein Eng Des Sel.* 2009;22(3):169-74.
106. Vendel MC, Favis M, Snyder WB, Huang F, Capili AD, Dong J, et al. Secretion from bacterial versus mammalian cells yields a recombinant scFv with variable folding properties. *Arch Biochem Biophys.* 2012;526(2):188-93.
107. Supimon K, Sangsuwannukul T, Sujjittjoon J, Phanthaphol N, Chieochansin T, Pongvarin N, et al. Anti-mucin 1 chimeric antigen receptor T cells for adoptive T cell therapy of cholangiocarcinoma. *Scientific Reports.* 2021;11:1-14.
108. Richins RD, Kaneva I, Mulchandani A, Chen W. Biodegradation of organophosphorus pesticides by surface-expressed organophosphorus hydrolase. *Nature Biotechnology.* 1997;15:984-7.
109. Gallus S, Peschke T, Paulsen M, Burgahn T, Niemeyer CM, Rabe KS. Surface Display of Complex Enzymes by in Situ SpyCatcher-SpyTag Interaction. *Chembiochem.* 2020;21(15):2126-31.

110. Sharma J, Shepardson K, Johns LL, Wellham J, Avera J, Schwarz B, et al. A Self-Adjuvanted, Modular, Antigenic VLP for Rapid Response to Influenza Virus Variability. *ACS Appl Mater Interfaces*. 2020;12(16):18211-24.
111. Cai W, Kesavan DK, Wan J, Abdelaziz MH, Su Z, Xu H. Bacterial outer membrane vesicles, a potential vaccine candidate in interactions with host cells based. *Diagn Pathol*. 2018;13(1):95.
112. Zanella I, König E, Tomasi M, Gagliardi A, Frattini L, Fantappiè L, et al. Proteome-minimized outer membrane vesicles from *Escherichia coli* as a generalized vaccine platform. *J Extracell Vesicles*. 2021;10(4):e12066.
113. Akerström B, Nilsson BHK, Hoogenboom HR, Björck L. On the interaction between single chain Fv antibodies and bacterial immunoglobulin-binding proteins. *Journal of Immunological Methods*. 1994;177:151-63.
114. Kimple ME, Brill AL, Pasker RL. Overview of affinity tags for protein purification. *Curr Protoc Protein Sci*. 2013;73:9 1-9 23.





APPENDIX

จุฬาลงกรณ์มหาวิทยาลัย
CHULALONGKORN UNIVERSITY

APPENDIX

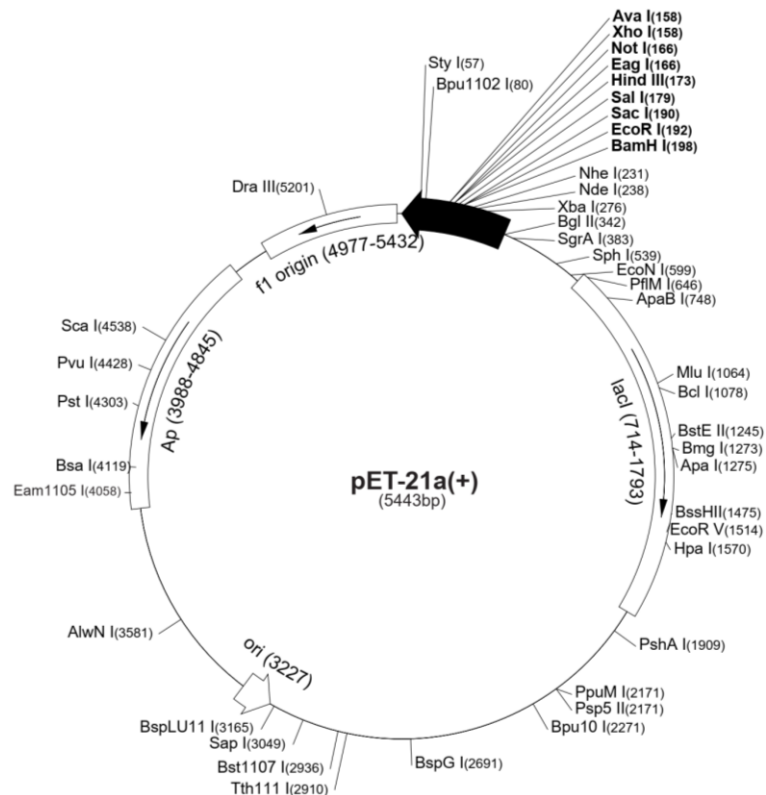


Figure 21 The circular map of pET21a+ vector

>LppOmpA+SpyCatcher

CATATGATGAAGGCGACCAAGTTAGTCCTGGGCGCTGTGATCCTCGGTTCTACGCTGCTTGCTGGTTG
 TAGCAGTAACGCGAAAATTGACCAGGGCATTAAATCCGTACGTCCGTTTCGAAATGGGCTACGATTGGT
 TGGGCCGTATGCCTTATAAAGGTTCTGTAGAGAACGGTGCGTATAAAGCCCAGGGCGTCCAGTTAAC
 GCGAAGCTCGGGTACCCCATCACTGATGATCTTGATATCTACACCCGGCTTGGTGGCATGGTGTGGCG
 CGCCGATACAAAAGAGCAATGTGTACGGTAAAAACCATGATACCCGGTGTAAAGCCCCGTGTTTGCGGGAG
 GTGTTGAGTACGCAATTACCCCGAAATTGCGACTCGTCTGGAATATCAATGGACCAATAACATCGGC
 GATGCACACACCATTGGTACGCGCCCGGATAACGGGGTG *GGGTC*GGCGGAAGCGGCG**GGATCC**CGCAT
 GGTGGACACGCTGAGCGGACTGTCCCTCGGAACAGGGTCAGTCTGGGGATATGACTATCGAAGAAGATT
 CCGCGACCCACATTAATTTCTCTAAACGTGATGAAGACGGTAAAGAATTAGCGGGTGCCACGATGGAA
 TTACGTGATTCTTCAGGTAAAACAATTAGTACGTGGATTTTCAGACGGACAAGTCAAGGATTTTTATCT
 CTATCCGGCAAATATACGTTTCGTAGAGACCGCGGCACCCGGATGGTTATGAGGTTGCTACTGCCATCA
 CATTACCGTGAACGAGCAGGGCCAGGTGACCGTTAATGGGAAAGCGACAAAGGGGGATGCTCATATC
 GGTAGCGGCGGTTTCAGGG **CATCACCATCATCACCCTGA**GAATTC

>LppOmpA+SpyCatcher

HMMKATKLVLGAVILGSTLLAGCSSNAKIDQGINPYVGFEMGYDNLGRMPYKGSVENGAYKAQGVQLT
 AKLGYPITDDLDIYTRLGGMVWRADTKSNVYGKNHDTGVSPVFAGGVEYAITPEIATRLEYQWTNNIG
 DAHTIGTRPDNGV *GSGGSGGS*AMVDTL SGLSSEQQSGDMTIEEDSATHIKFSKRDEDGKELAGATME
 LRDSSGKTI STWISDGQVKDFYLYPGKYTFVETAAPDGYEVATAITFTVNEQGQVTVNGKATKGDALH
 GSGGSG **HHHHH***

Figure 22 Sequence of gene cassette encoding Lpp'OmpA-SpyCatcher fusion protein (top) and translated amino acid sequence (bottom). Restriction recognition sites inducing NdeI (5' CATATG 3'), BamHI (5' GGATCC 3'), and EcoRI (5' GAATTC 3') are shown as bold. GS-linkers are italic. Encoding genes are indicated in colors: lpp' ompa (yellow), spycatcher (blue), and histidine-tag (green). An asterisk indicates a stop codon.

```

LppOmpA+SC      1  -----
Seq+cIn.3      1  GGGGGCGGAAACATTCCTCTAGAATAATTTTGTTTAACTTTAAGAAGGAGATATACAT

LppOmpA+SC      1  ---CATATGATGAAGGCGACCAAGTTAGTCCTGGGCGCTGTGATCCTCGGTTCTACGCTG
Seq+cIn.3      61  AACCATATGATGAAGGCGACCAAGTTAGTCCTGGGCGCTGTGATCCTCGGTTCTACGCTG

LppOmpA+SC      58  CTTGCTGGTTGTAGCAGTAACGCGAAAAATTGACCAGGGCATTAAATCCGTACGTGGTTTC
Seq+cIn.3     121  CTTGCTGGTTGTAGCAGTAACGCGAAAAATTGACCAGGGCATTAAATCCGTACGTGGTTTC

LppOmpA+SC     118  GAAATGGGCTACGATTGGTTGGGCCGTATGCCTTATAAAGGTTCTGTAGAGAACGGTGCG
Seq+cIn.3     181  GAAATGGGCTACGATTGGTTGGGCCGTATGCCTTATAAAGGTTCTGTAGAGAACGGTGCG

LppOmpA+SC     178  TATAAAGCCAGGGCGTCCAGTTAACCGCGAAGCTCGGGTACCCCATCACTGATGATCTT
Seq+cIn.3     241  TATAAAGCCAGGGCGTCCAGTTAACCGCGAAGCTCGGGTACCCCATCACTGATGATCTT

LppOmpA+SC     238  GATATCTACACCCGGCTTGGTGGCATGGTGTGGCGCGCCGATACAAGAGCAATGTGTAC
Seq+cIn.3     301  GATATCTACACCCGGCTTGGTGGCATGGTGTGGCGCGCCGATACAAGAGCAATGTGTAC

LppOmpA+SC     298  GGTA AAAACCATGATACCGGTGTAAGCCCGGTGTTTGGGGAGGTGTTGAGTACGCAATT
Seq+cIn.3     361  GGTA AAAACCATGATACCGGTGTAAGCCCGGTGTTTGGGGAGGTGTTGAGTACGCAATT

LppOmpA+SC     358  ACCCCGAAATTCGACTCGTCTGGAATATCAATGGACCAATAACATCGGCGATGCACAC
Seq+cIn.3     421  ACCCCGAAATTCGACTCGTCTGGAATATCAATGGACCAATAACATCGGCGATGCACAC

LppOmpA+SC     418  ACCATTGGTACGCGCCCGGATAACGGGGTGGGGTCTGGCGGAAGCGGGGATCCGCGATG
Seq+cIn.3     481  ACCATTGGTACGCGCCCGGATAACGGGGTGGGGTCTGGCGGAAGCGGGGATCCGCGATG

LppOmpA+SC     478  GTGGACACGCTGAGCGGACTGTCCCTCGGAACAGGGTCAGTCTGGGGATATGACTATCGAA
Seq+cIn.3     541  GTGGACACGCTGAGCGGACTGTCCCTCGGAACAGGGTCAGTCTGGGGATATGACTATCGAA

LppOmpA+SC     538  GAAGATTCCGCGACCCACATTAATTCCTAAACGTGATGAAGACGGTAAAGAATTAGCG
Seq+cIn.3     601  GAAGATTCCGCGACCCACATTAATTCCTAAACGTGATGAAGACGGTAAAGAATTAGCG

LppOmpA+SC     598  GGTGCCAGATGGAATTACGTGATCTTCAGGTAAAACAATTAGTACGTGGATTTACAGC
Seq+cIn.3     661  GGTGCCAGATGGAATTACGTGATCTTCAGGTAAAACAATTAGTACGTGGATTTACAGC

LppOmpA+SC     658  GGACAAGTCAAGGATTTTATCTCTATCCGGCAAAATATACGTTGTTAGAGACCGCGCA
Seq+cIn.3     721  GGACAAGTCAAGGATTTTATCTCTATCCGGCAAAATATACGTTGTTAGAGACCGCGCA

LppOmpA+SC     718  CCGGATGGTTATGAGGTTGCTACTGCCATCACATTTACCCTGAACGAGCAGGGCCAGGTG
Seq+cIn.3     781  CCGGATGGTTATGAGGTTGCTACTGCCATCACATTTACCCTGAACGAGCAGGGCCAGGTG

LppOmpA+SC     778  ACCGTTAATGGGAAAGCGACAAAGGGGGATGCTCATATCGGTAGCGGGGTTACGGGCAT
Seq+cIn.3     841  ACCGTTAATGGGAAAGCGACAAAGGGGGATGCTCATATCGGTAGCGGGGTTACGGGCAT

LppOmpA+SC     838  CACCATCATCACCCTGAGAATTC-----
Seq+cIn.3     901  CACCATCATCACCCTGAGAATTCGAGTCCGTCGACAAGCTTGGGGCCGACTCGAGCA

LppOmpA+SC     961  -----
Seq+cIn.3     961  CCACCACCACCACCCTGAGATCCGGCTGTAACAAGCCCGAAAGGAAGCTGAGTTGGC

LppOmpA+SC    1021  -----
Seq+cIn.3    1021  TGCTGCCACCCTGAGCAATAACTAGCATAACCCCTGGGGCCCCATAACGGGCCTTGAG

LppOmpA+SC    1081  -----
Seq+cIn.3    1081  GGGTTTTTGCCTAAAGGAGGAAGCTTAATCCGGATTGGCGAATGGGACCGC

```

Figure 23 DNA sequence alignment of designed Lpp'OmpA-SpyCatcher sequence (LppOmpA+SC) and sequencing read from clone number 3 (Seq+cIn.3). This alignment was performed using ClustalW2 pairwise method by T-Coffee (<http://tcoffee.org.cat/apps/tcoffee/>) and adjusted to readable format by BoxShade (http://www.ch.embnet.org/software/BOX_form.html).

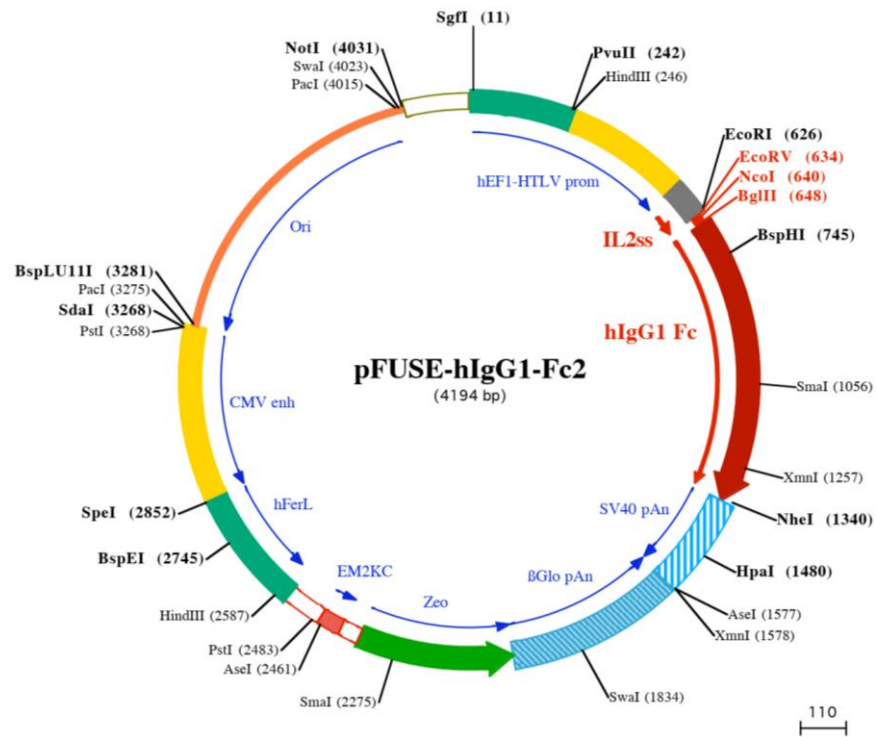
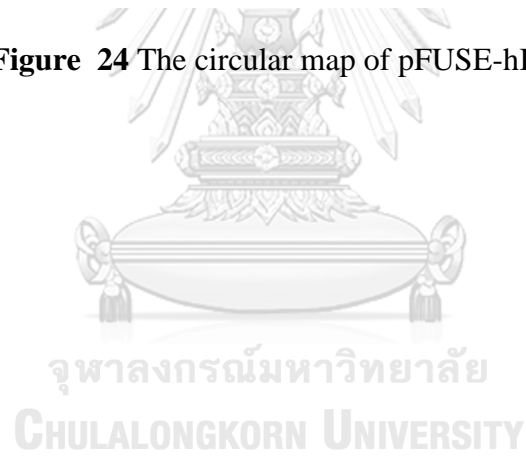


Figure 24 The circular map of pFUSE-hIgG1-Fc2



>SpyCatcher+SM3

```

ATGTACAGGATGCAACTCCTGTCTTGCATTGCACTAAGTCTTGCACCTTGTACGAATTCGCACCACCA
TCACCACCAGGGCGGCTCCGGTTCAGATCGATACTCTTTCTGGCCTCAGCTCAGAGCAAGGCCAGTCCG
GCGATATGACCATTGAGGAAGATAGCGCAACACACATCAAGTTCTCTAAACGGGACGAAGATGGCAA
GAATTGGCTGGGGCCACTATGGAAGTGCCTGACAGCAGCGGTAAGACAATTAGCACCTGGATCTCAGA
CGGTCAAGTGAAAGATTTTTACCTATATCCCAGTAAGTACACCTTTGTGGAAACTGCCGCACCGGATG
GCTATGAAGTTGCAACCGCCATCACATTTACTGTGAACGAGCAGGGCCAGGTCACCGTGAATGGCAAG
GCAACCAAGGGGGACGCTCATATCGGCTCCGGTACTGCTGGCGGGGGAGCGGGTCTAGATCTCAGGT
GCAGCTCCAAGAGAGCGGAGGAGGACTGGTACAGCCCAGGAGGCTCAATGAAGCTCAGCTGCGTGCCTT
CTGGATTTACATTCTCTAATTACTGGATGAACTGGGTACAGACAGTCACCGGAGAAAGGTCTTGAGTGG
GTGGCCGAGATACGGTTGAAGTCCAACAACACTACGCAACCCATTACGCAGAGAGCGTTAAAGGCCGATT
CACAATCTCTAGGGACGATTCCAAGAGTAGTGTCTATCTCCAGATGAACAATCTAAGAGCCGAGGACA
CTGGTATCTACTACTGTACAGGAGTTGGCCAGTTCGCCTACTGGGGCCAGGGGACCCTGTGACCGTG
TCATCCTCTTCTGGAGGCGGCGGCTCCGGAGGAGGAGGGGATCCTCAGGCAGCTCAGACATCGTGGT
TACTCAGGAGTCCGCCCTGACAACCAGCCCTGGTGAACCGGTCACTCTGACCTGTAGGAGCAGTACAG
GGGCTGTGACGACTTCTAACTATGCCAATTGGGTGCAGGAGAAGCCTGATCATCTGTTTACCGGTCTG
ATCGGCGGGACTAACAATCGTGCACCTGGCGTTCCTGCCAGATTTAGCGGCTCTCTAATCGGAGATAA
AGCCGCATTGACTATCACGGGCGCCAAACAGAGGATGAGGCCATCTATTTCTGCGCACTGTGGTACA
GCAACCACTGGGTGTTTGGGGGGGCACAAAACACTGACTGTCTCTGGGTTGAGTGCTAGC

```

>dsDNA_for_SpyTag+SM3

```

CTTGCACCTTGTACGAATTCGCATCACCATCATCCCATGGCAGCGGGGGCTCAGGCGCCACATTGT
GATGGTGGACGCCTACAAACCTACCAAGGGCTCCGGTACTGCTGGCGGGGGAGCGGGTCTAGATCTC
AGGTGCAGCTCCAA

```

Figure 25 DNA sequences of genes used in Gibson assembly for construction of pSpyTag-SM3 including gene encoding SpyCatcher-SM3 in pSpyCatcher-SM3 (top) and a double stranded DNA containing spytag gene (bottom). (Top) The spycatcher gene highlighted in magenta was cut by EcoRI and BglII and subsequently replaced by spytag gene from the synthetic double stranded DNA using Gibson cloning method. Other coding genes are listed in color: IL-2 signal sequence (grey) Histidine-tag (green), V_H of scFv clone SM3 (blue), and V_L of scFv clone SM3 (red). All restriction enzyme cut sites including EcoRI (5' GAATTC 3'), BglII (5' AGATCT 3'), and NheI (5' GCTAGC 3') are shown in bold and GS-linker sequence is presented in italic. (Bottom) The synthetic double stranded DNA is comprised of codon-optimized spytag gene (yellow) and histidine-tag (green) flanked by GS-linker (italic). A 20-bp overlapping sequence which matches to pSpyCatcher-SM3 at EcoRI and BglII recognition sites is shown underlined.

>SpyTag+SM3

```

ATGTACAGGATGCAACTCCTGTCTTGCATTGCACTAAGTCTTGCACCTTGTACGAATTCGCATCACCA
TCATCACCATGGCAGCGGGGGCTCAGGCGCCACATTGTGATGGTGGACGCCTACAAACCTACCAAGG
GCTCCGGTACTGCTGGCGGGGGGAGCGGGTCTAGATCTCAGGTGCAGCTCCAAGAGAGCGGAGGAGGA
CTGGTACAGCCCCGAGGCTCAATGAAGCTCAGCTGCGTCGCTTCTGGATTTACATTCTCTAATTACTG
GATGAACTGGGTCAGACAGTCACCGGAGAAAGGTCTTGAGTGGGTGGCCGAGATACGGTTGAAGTCCA
ACAACTACGCAACCCATTACGCAGAGAGCGTTAAAGGCCGATTCACAATCTCTAGGGACGATTCCAAG
AGTAGTGTCTATCTCCAGATGAACAATCTAAGAGCCGAGGACACTGGTATCTACTACTGTACAGGAGT
TGGCCAGTTTCGCTACTGGGGCCAGGGGACCCTGTGACCGTGTCATCCTCTTCTGGAGGCGGCGGCT
CCGGAGGAGGAGGGGATCCTCAGGCAGCTCAGACATCGTGGTTACTCAGGAGTCCGCCCTGACAACC
AGCCCTGGTGAAACGGTCACTCTGACCTGTAGGAGCAGTACAGGGGCTGTGACGACTTCTAACTATGC
CAATTGGGTGCAGGAGAAGCCTGATCATCTGTTTACCGGTCTGATCGGCGGGACTAACAATCGTGCAC
CTGGCGTTCCTGCCAGATTTAGCGGCTCTCTAATCGGAGATAAAGCCGCATTGACTATCACGGGCGCC
CAAACAGAGGATGAGGCCATCTATTTCTGCGCACTGTGGTACAGCAACCACTGGGTGTTTGGGGGGG
CACAAAACTGACTGTCCTGGGTTGAGTGCTAGC

```

>SpyTag+SM3

```

MYRMQLLSICIALSLALVTNSHHHHHHGSSGSAHIVMVDAYKPTKGSGTAGGSGSRSQVQLQESGGG
LVQPGGSMKLSCVASGFTFSNYWMNWVRQSPEKGLEWVAEIRLKSNNYATHYAESVKGRFTISRDDSK
SSVYLQMNLRAEDTGIYYCTGVGQFAYWGQGTTVTVSSSSGGGSGGGGSSGSDIVVTQESALTT
SPGETVTLTCRSSTGAVTTSNYANWVQEKPDHLFTGLIGGTNNRAPGVPARFSGSLIGDKAALTITGA
QTEDEAIYFCALWYSNHWFVGGGTKLTVLG*

```

Figure 26 SpyTag-SM3 DNA coding sequence and amino acid sequence. (Top) Coding genes are shown in color: IL-2 signal sequence (grey), Histidine-tag (green), spytag (yellow), V_H of scFv SM3 (blue), and V_L of scFv SM3 (red). GS-linkers are displayed in italic. All restriction enzyme cut sites including EcoRI (5' GAATTC 3'), BglIII (5' AGATCT 3'), and NheI (5' GCTAGC 3') are shown in bold. (Bottom) Translated amino acid of SpyTag-SM3. Details are same as described in DNA sequence. An asterisk points a stop codon.

```

SpyTag+SM3      1  -----
Seq+cln.13     1  TCTTTTCTCGGTTCTGCGGTTACAGATCCAAGCTGTGACCGGGCGCTACCTGAGATCA

SpyTag+SM3      1  -----ATGTACAGGATGCAACTCCTGTCTTGCATTGCACTAAGTCT
Seq+cln.13     61  CCGGCGAAGGAGGGCCACCATGTACAGGATGCAACTCCTGTCTTGCATTGCACTAAGTCT

SpyTag+SM3      42  TGCACCTTGTACGAATTCGCATCACCATCATCACCATGGCAGCGGGGGCTCAGGCGCCCA
Seq+cln.13     121  TGCACCTTGTACGAATTCGCATCACCATCATCACCATGGCAGCGGGGGCTCAGGCGCCCA

SpyTag+SM3      102  CATTGTGATGGTGGACGCTACAAACCTACCAAGGGCTCCGGTACTGCTGGCGGGGGGAG
Seq+cln.13     181  CATTGTGATGGTGGACGCTACAAACCTACCAAGGGCTCCGGTACTGCTGGCGGGGGGAG

SpyTag+SM3      162  CGGGTCTAGATCTCAGGTGCAGCTCCAAGAGAGCGGAGGAGACTGGTACAGCCCGGAGG
Seq+cln.13     241  CGGGTCTAGATCTCAGGTGCAGCTCCAAGAGAGCGGAGGAGACTGGTACAGCCCGGAGG

SpyTag+SM3      222  CTCAATGAAGCTCAGCTGCGTGCCTTCTGGATTTACATTTCTAATTACTGGATGAAGTGC
Seq+cln.13     301  CTCAATGAAGCTCAGCTGCGTGCCTTCTGGATTTACATTTCTAATTACTGGATGAAGTGC

SpyTag+SM3      282  GGTACAGACAGTCACCGGAGAAAGGCTTTGAGTGGGTGGCCGAGATACGGTTGAAGTCCAA
Seq+cln.13     361  GGTACAGACAGTCACCGGAGAAAGGCTTTGAGTGGGTGGCCGAGATACGGTTGAAGTCCAA

SpyTag+SM3      342  CAACTACGCAACCCATTACGCAGAGAGCGTTAAAGGCCGATTACAAATCTCTAGGGACGA
Seq+cln.13     421  CAACTACGCAACCCATTACGCAGAGAGCGTTAAAGGCCGATTACAAATCTCTAGGGACGA

SpyTag+SM3      402  TTCCAAGAGTAGTGTCTATCTCCAGATGAACAATCTAAGAGCCGAGGACACTGGTATCTA
Seq+cln.13     481  TTCCAAGAGTAGTGTCTATCTCCAGATGAACAATCTAAGAGCCGAGGACACTGGTATCTA

SpyTag+SM3      462  CTACTGTACAGGAGTTGGCCAGTTCGCCTACTGGGGCCAGGGGACCACTGTGACCGTGTG
Seq+cln.13     541  CTACTGTACAGGAGTTGGCCAGTTCGCCTACTGGGGCCAGGGGACCACTGTGACCGTGTG

SpyTag+SM3      522  ATCCTCTTCTGGAGGGCGGGCTCCGGAGGAGGAGGGGGATCCTCAGGCAGCTCAGACAT
Seq+cln.13     601  ATCCTCTTCTGGAGGGCGGGCTCCGGAGGAGGAGGGGGATCCTCAGGCAGCTCAGACAT

SpyTag+SM3      582  CGTGGTACTCAGGAGTCCGCCCTGACAACCAGCCCTGGTGAACCGTCACTCTGACCTG
Seq+cln.13     661  CGTGGTACTCAGGAGTCCGCCCTGACAACCAGCCCTGGTGAACCGTCACTCTGACCTG

SpyTag+SM3      642  TAGGAGCAGTACAGGGGCTGTGACGACTTCTAACTATGCCAATTGGGTGCAGGAGAAGCC
Seq+cln.13     721  TAGGAGCAGTACAGGGGCTGTGACGACTTCTAACTATGCCAATTGGGTGCAGGAGAAGCC

SpyTag+SM3      702  TGATCATCTGTTTACCGGTCTGATCGGCGGGACTAACAATCGTGCACCTGGCGTTCCTGC
Seq+cln.13     781  TGATCATCTGTTTACCGGTCTGATCGGCGGGACTAACAATCGTGCACCTGGCGTTCCTGC

SpyTag+SM3      762  CAGATTTAGCGGCTCTCTAATCGGAGATAAAGCCGCATTGACTATCACGGGCGCCAAAC
Seq+cln.13     841  CAGATTTAGCGGCTCTCTAATCGGAGATAAAGCCGCATTGACTATCACGGGCGCCAAAC

SpyTag+SM3      822  AGAGGATGAGGCCATCTATTTCTGCGCACTGGTACAGCAACCAC TGGGTGTTTGGGGG
Seq+cln.13     901  AGAGGATGAGGCCATCTATTTCTGCGCACTGGTACAGCAACCAC TGGGTGTTTGGGGG

SpyTag+SM3      882  GGGCACA AAACTGACTGTCCTGGGTTGAGTGCTAGC-----
Seq+cln.13     961  GGGCACA AAACTGACTGTCCTGGGTTGAGTGCTAGCTGGCCAGACATGATAAGATACATT

SpyTag+SM3      -----
Seq+cln.13     1021  GATGAGTTTGGACAAAACCACAAC TAGAATGCAGTGA AAAAAATGCTTTATTTTGTGAAAT

SpyTag+SM3      -----
Seq+cln.13     1081  TTGTGATGCTATTGCTTTATTTGTAACCATTA AA

```

Figure 27 DNA alignment of sequencing read from recombinant pSpyTag-SM3 clone number 13 and SpyTag-SM3 sequence. This alignment was performed as previously described in figure 23.

VITA

NAME SEDTHAWUT LAOTEE

DATE OF BIRTH 23 JANUARY 1997

PLACE OF BIRTH SRAKAEW, THAILAND

INSTITUTIONS ATTENDED BACHELOR OF SCIENCE, DEPARTMENT OF BIOCHEMISTRY, FACULTY OF SCIENCE, CHULALONGKORN UNIVERSITY

HOME ADDRESS 16/2, MOO 2, BANGPOR, MUANGNARATHIWAT, NARATHIWAT, 96000



จุฬาลงกรณ์มหาวิทยาลัย
CHULALONGKORN UNIVERSITY